

1 Evaluation of precipitation estimates over CONUS derived from satellite,
2 radar, and rain gauge datasets at daily to annual scales (2002-2012)

3

4

5 Olivier P. Prat^{1,*}, and Brian R. Nelson²

6

7

8 ¹Cooperative Institute for Climate and Satellites-NC (CICS-NC), North Carolina State
9 University, and NOAA/National Climatic Data Center, Asheville, NC

10 ²Remote Sensing Applications Division (RSAD), NOAA/NESDIS/NCDC, Asheville, NC

11

12 *Second Revised Version Submitted to Hydrology and Earth System Sciences*

13 *Special Issue: Precipitation: measurement and space-time variability*

14

April 2015

15

16 *Corresponding author:

17 Dr. Olivier P. Prat

18 Cooperative Institute for Climate and Satellites-NC (CICS-NC)

19 North Carolina State University and NOAA/National Climatic Data Center

20 151 Patton Ave.

21 Asheville, NC 28801, USA

22 Phone: +1-828-257-3141

23 Email: olivier.prat@noaa.gov

1 ABSTRACT

2 We use a suite of quantitative precipitation estimates (QPEs) derived from satellite, radar,
3 and surface observations to derive precipitation characteristics over CONUS for the
4 period 2002-2012. This comparison effort includes satellite multi-sensor datasets (bias-
5 adjusted TMPA 3B42, near-real time 3B42RT), radar estimates (NCEP Stage IV), and
6 rain gauge observations. Remotely sensed precipitation datasets are compared with
7 surface observations from the Global Historical Climatology Network (GHCN-Daily)
8 and from the PRISM (Parameter-elevation Regressions on Independent Slopes Model).
9 The comparisons are performed at the annual, seasonal, and daily scales over the River
10 Forecast Centers (RFCs) for CONUS. Annual average rain rates present a satisfying
11 agreement with GHCN-D for all products over CONUS ($\pm 6\%$). However, differences at
12 the RFC are more important in particular for near-real time 3B42RT precipitation
13 estimates (-33% to +49%). At annual and seasonal scales, the bias-adjusted 3B42
14 presented important improvement when compared to its near real time counterpart
15 3B42RT. However, large biases remained for 3B42 over the Western US for higher
16 average accumulation (≥ 5 mm/day) with respect to GHCN-D surface observations. At
17 the daily scale, 3B42RT performed poorly in capturing extreme daily precipitation (> 4 in
18 day^{-1}) over the Northwest. Furthermore, the conditional analysis and a contingency
19 analysis conducted illustrated the challenge in retrieving extreme precipitation from
20 remote sensing estimates.

1 **1. Introduction**

2 Over the last decades, numerous long-term rainfall datasets were developed using
3 rain gauge (RG) precipitation measurements, remotely sensed (ground based radars,
4 satellites) quantitative precipitation estimates (QPE), or combining different sensors, each
5 of which have specific characteristics and limitations. Extensive information on
6 precipitation measurement methodologies and available precipitation products can be
7 found in Michaelides et al. (2009), Kidd et al. (2010), and Tapiador et al. (2012) among
8 others. One of the limitations in using rain gauge based precipitation datasets lies in the
9 fact that the geographical coverage is not spatially homogeneous. By contrast, multi-
10 sensor satellite-based products: PERSIANN (Precipitation Estimation from Remotely
11 Sensed Information using Artificial Neural Networks: Sorooshian et al. 2000) and
12 variants PERSIANN-CDR (Climate Data Record: Ashouri et al. 2015), CMORPH (CPC
13 MORPHing technique: Joyce et al. 2004), and TRMM (Tropical Rainfall Measuring
14 Mission) TMPA (TRMM Multisatellite Precipitation Analysis: Huffman et al. 2007) or
15 ground-based radar rainfall estimates: NCEP (National Centers for Environmental
16 Prediction) Stage IV (Lin and Mitchell 2005) or more recently the National Mosaic and
17 Multi-sensor QPE (NMQ/Q2) (Zhang et al. 2011), provide an opportunity to broach the
18 problem of sparse observations over land and/or ocean. Precipitation datasets at high
19 spatial (typically 4-25 km) and temporal (1-6h) resolution allow for assessing annual,
20 seasonal, and daily characteristics of precipitation at local, regional, and continental
21 scales (Huffman et al. 2001, Sorooshian et al. 2002, Nesbitt and Zipser 2003, Liu and
22 Zipser 2008, Nesbitt and Anders 2007, Sapiano and Arkin 2009, Prat and Barros 2010a,
23 Sahany et al. 2010, Kidd et al. 2012, Prat and Nelson 2013a,b, 2014 among others).

1 The purpose of this study is to evaluate the ability of QPE products to describe
2 precipitation patterns and capture precipitation extremes over a multi-annual time frame.
3 While a lot of studies are available that compared different radar/satellite products on an
4 event-to-event basis, in this work we focus on the long-term perspective (11 years). The
5 objective of this study is to provide a comparison of a suite of common Quantitative
6 Precipitation Estimates derived from satellites, radars, and rain gauges datasets for the
7 period 2002-2012 over CONUS. Our aim is to evaluate the ability of satellite (TMPA
8 3B42, 3B42RT) and ground-based remotely sensed (Stage IV) precipitation products to
9 describe precipitation patterns. In particular, we will investigate how the different QPE
10 products compare with respect to long-term surface observations and what are the
11 associated uncertainties. The choice of 3B42 is guided by the fact that a monthly
12 accumulation adjustment is performed on the near-real time algorithm 3B42RT and thus
13 provides bias-adjusted precipitation estimates when compared to non-adjusted versions of
14 CMORPH and PERSIANN. Furthermore, there are a fair amount of studies available
15 that compare the respective merit of the datasets described above either against each
16 other or against other datasets used as reference. Those studies often investigate isolated
17 events such as intense precipitation or focus on a time period that is limited by day,
18 month, or season. It is seldom that studies that deal with the long-term assessment of
19 precipitation products (annual or multi-annual basis) are available in the scientific
20 literature (Chen et al. 2013). The remotely sensed datasets will be compared against
21 surface observations from the Global Historical Climatology Network (GHCN-Daily)
22 and estimations from the Parameter-elevation Regressions on Independent Slopes Model
23 (PRISM), which combines surface observations with a digital elevation model to account

1 for the orographic enhancement of precipitation. Both GHCN-D and PRISM will be used
2 as a baseline for QPE products evaluations. The study will analyze 11 years (2002-2012)
3 of rainfall data over CONUS. The duration of the study will allow the assessment of
4 systematic biases, and capture year-to-year and seasonal variability. In addition to long-
5 term average precipitation characteristics, we will investigate the ability for each of those
6 QPE products to capture extreme events and how they compare with surface
7 observations.

8 The paper is organized as follows: In the first section, we present briefly the
9 precipitation datasets used in this study. In the second section, we will present a
10 comparison between precipitation estimates at the annual and seasonal scales. In the
11 third part, we will investigate the impact of differing spatial and temporal resolutions
12 with respect to the datasets' ability to capture extreme precipitation events. Finally, the
13 paper summarizes the major results of this study.

14

15 **2. Precipitation datasets and algorithms description**

16 In this section, we provide a brief description of these different precipitation
17 datasets used. The interested reader will refer to the references cited.

18

19 2.1 – Rain gauge precipitation datasets: GHCN-Daily

20 Precipitation surface observations are taken from the Global Historical
21 Climatology Network-Daily (GHCN-D). The dataset gathers records from over 80,000
22 stations over 180 countries. About two-thirds of those stations report total daily
23 precipitation only and other stations include additional information such as maximum and

1 minimum temperature, snowfall, and snow depth (Menne et al. 2012). The entire dataset
2 is routinely quality controlled to ensure basic consistency. The GHCN-D dataset
3 incorporates surface observations from different sources (see Table 2 in Menne et al.
4 2012). We selected the subset from the US-Cooperative Observing network (US-COOP),
5 which represented about 9000 stations. The US-COOP network includes first order
6 stations (1600 manual and automatic synoptic stations) and stations from volunteer
7 observers. Figure 1a presents the location of the 8815 surface observations in the
8 GHCN-D database over CONUS. For the current study, only the 4075 rain gauges
9 reporting at least 90% of the time during the period 2002-2012 are selected to ensure
10 stable statistics (Figure 1b). Although there is a 50% decrease in the total number of rain
11 gauges, the remaining rain gauges conserved a comparable spatial distribution than the
12 original network and the removed gauges were evenly distributed throughout CONUS.
13 The surface stations are compared with the nearest pixel of the gridded precipitation
14 estimates derived from the selected datasets (PRISM, Stage IV, 3B42, 3B42RT)
15 described below.

16

17 2.2 – Rain gauge gridded precipitation datasets: PRISM

18 The PRISM algorithm (available at <http://www.prism.oregonstate.edu/>) combines
19 point data with a digital elevation model to generate gridded estimates of precipitation
20 along with a suite of climatological variables such as temperature, snowfall, and degree
21 dew point among others (Daly et al. 1994). Data are available at the daily, monthly, and
22 annual scale and at various spatial resolutions (800m to 4km). In this work, we use the
23 monthly precipitation estimates at the 4-km nominal spatial resolution (dataset AN81m:

1 PRISM Technical Note 2014). The PRISM precipitation estimates incorporate surface
2 data observations from GHCN-D among others. The systematic comparison of point
3 surface observations from GHCN-D and gridded estimates from PRISM will be
4 performed as a consistency check. The PRISM precipitation estimates will be used as a
5 baseline data set to evaluate remotely sensed precipitation products (Stage IV, 3B42,
6 3B42RT) at the annual and seasonal scale.

7

8 2.3 – Radar precipitation datasets: the Stage IV analysis

9 The NCEP Stage IV product, herein referred to as Stage IV, is a near real time
10 product that is generated at NCEP separately from the NWS Precipitation Processing
11 System (PPS) and the NWS River Forecast Center (RFC) rainfall processing. Originally
12 the Stage IV product was intended for assimilation into atmospheric forecast models to
13 improve quantitative precipitation forecasts (QPF) (Lin and Mitchell 2005). However the
14 length of record, consistency of data availability, and ease of access has made the Stage
15 IV product attractive for many applications. Data are available in GRIB format for
16 hourly, 6-hourly, and daily temporal scales and they are gridded on the Hydrologic
17 Rainfall Analysis Projection (HRAP) (Reed and Maidment 1995, 1999) at a nominal 4-
18 km spatial resolution. Stage IV represents the final stage of the process that combines
19 mosaicked estimates from the 12 RCFs. The gauges used at the RFC level for bias-
20 adjustment include available hourly rain gauges such as HADS (Hydrometeorological
21 Automated Data System) gauges, ASOS (Automated Surface Observing System), and
22 AWOS (Automated Airport Weather Stations) reports (Hou et al. 2014). Furthermore,
23 some of the Western RCFs (Colorado Basin River: CBRFC, California-Nevada: CNRFC,

1 Northwestern: NWRFC) do not use radar estimates due to poor coverage over
2 mountainous areas. Those RFCs use an automated analysis of rain gauge observations
3 (Mountain Mapper) that incorporates the gridded monthly precipitation climatology from
4 PRISM. Although changes in gauge-adjustments procedures are always possible at the
5 RFC level including the incorporation of the best available in-situ observations, it is
6 reasonable to assume that the in-situ observations used in the Stage IV bias-adjustment
7 procedure (HADS, ASOS, AWOS) are different from the US-COOP subset of GHCN-D
8 used for the evaluation. For the Western RFCs however, the incorporation of the PRISM
9 climatology that uses GHCN-D in-situ data will have to be kept in mind for any analysis.
10 Figure 1c presents the geographical extent of the 12 RFCs and Table 1 reports the
11 number of available rain gauges by RFC. The Stage IV precipitation data are available
12 via: (<http://data.eol.ucar.edu/codiac/dss/id=21.093>). The reader will find a more detailed
13 description of the Stage IV precipitation retrievals from the RFC level and up to the final
14 mosaicked product in Nelson et al. (2015). In addition to radar only reflectivity scanning
15 and processing (beam blockage, hot and cold biases, bright-band contamination,
16 anomalous propagation, cone of silence), the final mosaicked estimates present biases
17 that are visible in the long-term averages. The fact that not all the RFCs use the same
18 precipitation estimation algorithm generates radar-to-radar and RFC-to-RFC
19 discontinuities (Nelson et al. 2015).

20

21 2.4 – Satellite precipitation QPE datasets: TMPA 3B42 and 3B42RT

22 The satellite QPE TMPA 3B42 Version 7 (V7) blends optimally different
23 microwave datasets from low earth orbit satellites (TMI: The Microwave Imager; SSM/I:

1 Special Sensor Microwave Imager; AMSR-E: Advanced Micro-wave Scanning
2 Radiometer-Earth Observing System; AMSU-B: Advanced Microwave Sounding Unit-
3 B), along with calibrated IR estimates of rain gauge corrected monthly accumulation
4 (Huffman et al. 2007). TMPA 3B42 provides precipitation estimates for the domain
5 50°S–50°N at a 3-hourly and quarter degree resolution (0.25°x0.25°) from which
6 seasonal, daily, and sub-daily precipitation characteristics can be derived. The quality of
7 the blended precipitation estimates depends on the number of satellite estimates available
8 at a given time stamp and on the sensor characteristics. Over the years, the retrieval
9 algorithms of the different products incorporated within 3B42 were modified. The
10 algorithm 3B42 itself had several versions and a major improvement of the precipitation
11 estimates was provided in 2007 to correct for low biases (Huffman et al., 2007). The
12 3B42 V7 represents substantial improvement when compared to the previous version
13 (V6). The version 7 incorporates additional satellite products along with the reprocessed
14 versions of the merged algorithms (TMI, SSM/I, AMSR-E, AMSU-B). However, the
15 major upgrade consists of the use of a single, uniformly processed surface precipitation
16 gauge analysis from the Global Precipitation Climatology Centre (GPCC) (Huffman and
17 Bolvin 2013). The gauge analysis used is the GPCC Monitoring Product at 1-deg grid
18 resolution (Schneider et al., 2010, 2011). This specific analysis uses SYNOP (synoptic
19 weather observation reports) and CLIMAT reports that are received near-real time from
20 7000-8000 automated stations worldwide. While it is possible that some of the first order
21 automated synoptic stations included in GHCN-D are also used in the GPCC gauge
22 analysis (SYNOP), most of the US-COOP subset of the GHCN-D stations used for
23 evaluation are not a part of the GPCC Monitoring Product used in the 3B42. Being

1 virtually impossible to track down and identify the automated stations that are or are not
2 used in the bias-adjustment procedure for 3B42, we are confident that this number
3 remaining relatively low will not compromise the independent assessment of the 3B42
4 dataset. The use of the GPCC rain gauge analysis explains most of the differences
5 observed between V6 and V7 over land and over coastal areas. A brief comparison of
6 both versions was provided for the period 1998-2009 over North and Central America,
7 which encompasses the current CONUS domain, in Prat and Nelson 2013b (see Figure
8 B1). In this work, we also use the near real time version of the product (3B42RT), which
9 is produced operationally and does not use the monthly rain gauge correction (GPCC) but
10 incorporates an a-priori climatological correction (Huffman et al., 2007). In addition to
11 products relying on gauge measurements (GHCN-D, PRISM) and incorporating gauge
12 information for bias adjustment purposes (Stage IV, TMPA 3B42), the use of the near
13 real time dataset 3B42RT has a double objective. First it provides a quantification of the
14 systematic biases and the adjustment performed with respect to surface observations.
15 Second, it aims to examine the suitability of satellite precipitation products to capture
16 precipitation patterns and extremes in near real time.

17

18 **3. Annual precipitation: differences between datasets**

19 3.1 – Annual average precipitation

20 Figure 2 displays the annual average precipitation derived from PRISM (Fig. 2a),
21 Stage IV (Fig. 2b), 3B42 (Fig. 2c), and 3B42RT (Fig. 2d) for the period 2002-2012. All
22 datasets present comparable precipitation patterns with higher rainfall east of 97°W, over
23 the southeast, and over the Pacific Northwest. Precipitation derived from Stage IV

1 displays a closer agreement with PRISM with comparable rainfall over the Northwest and
2 over the Rockies. The adjusted 3B42 presents a better visual agreement with PRISM and
3 Stage IV than the near real time version 3B42RT. However, rainfall over the Pacific
4 Northwest is noticeably lower than that retrieved from PRISM and Stage IV. The effect
5 of monthly accumulation correction between 3B42 and 3B42RT is particularly
6 conspicuous over the Northwest, the Rockies, and the Northeast. Over the Northeast, the
7 annual average precipitation differences between 3B42 and 3B42RT are above +2
8 mm/day. Annual average precipitation differences between bias-adjusted and non-
9 adjusted datasets are about +1 mm/day over the Northeast. Those differences are about -
10 1.5 mm/day over the Rockies. CONUS-wide the mean average annual precipitation for
11 the unadjusted 3B42RT is 2.62 mm/day; for 3B42 it is 2.54 mm/day (3% difference).

12

13 3.2 – Comparison with surface observations

14 To compare the different estimates for the annual average precipitation, we make
15 the assumption that each rain gauge represents with sufficient accuracy the area-averaged
16 rainfall over the native resolution of the different products evaluated: PRISM and Stage
17 IV (4x4-km²) and 3B42 and 3B42RT (4x4-km²). While, there are well known limitations
18 of using rain gauge point measurements to evaluate area-averaged rainfall retrieved from
19 sensors with coarser spatial resolution (Ciach and Krajewski 1999, Ciach et al. 2003,
20 Habib et al. 2004, Ciach et al. 2007), the random sampling errors due to differing
21 resolutions are mostly dominant at the sub-daily scales (Ciach and Krajewski 1999). For
22 accumulation period of several days the correlation distance (maximum distance between
23 stations beyond which the correlations become insignificant), is of the order of several

1 hundred kilometers (Gutowski et al. 2003). Those distances are several orders of
2 magnitude greater than the sensors spatial resolution.

3 Figure 3 displays the scatterplots along with the Q-Q (Quantile-Quantile) plots for
4 annual average precipitation derived from PRISM, Stage IV, 3B42, and 3B42RT when
5 compared to GHCN-D. Over CONUS (Fig. 3a), we observe a very good agreement
6 between GHCN-D surface observations and PRISM ($a=0.98$; $R^2=0.98$) as expected due to
7 the fact that PRISM gridded precipitation estimates incorporate GHCN-D stations.
8 Values for the mean annual average precipitation and the associated standard deviation
9 (σ) are relatively close at 2.42 mm/day ($\sigma = 1.11$ mm/day) for PRISM and 2.47 mm/day
10 ($\sigma = 1.14$ mm/day) for GHCN-D. The differences observed toward higher rain rates ($R >$
11 6 mm/day) are due to the algorithm that uses a digital elevation model and incorporates
12 complex precipitation processes such as rain shadows and coastal effects among others
13 (Daly et al. 1994). Comparison of Stage IV estimates with GHCN-D displays an overall
14 satisfying agreement ($a=0.93$; $R^2=0.93$) with lower precipitation estimates for Stage IV
15 for rain rates greater than 4 mm/day. The satellite QPEs (3B42, 3B42RT) display the
16 highest mean annual average precipitation over CONUS when compared to other
17 precipitation estimates (GHCN-D, PRISM, Stage IV) with 2.54 mm/day for 3B42 and
18 2.62 mm/day for 3B42RT along with a lower correlation coefficient (Fig. 3a). However,
19 while the mean annual average precipitation is higher than surface observations, 3B42
20 and 3B42RT display negative biases in the upper part of the distribution ($R > 4$ mm/day)
21 as revealed by the Q-Q plots. In addition, the bias-adjusted 3B42 presents a better
22 agreement with surface observations ($a=1.00$; $R^2=0.83$) than the near real time
23 precipitation estimates from 3B42RT ($a=0.99$; $R^2=0.36$). Overall, a better agreement is

1 found for Stage IV than for the satellite estimates (3B42, 3B42RT) in the upper part of
2 the distribution. The differences between surface observations (GHCN-D) and the
3 precipitation datasets (PRISM, Stage IV, 3B42, 3B42RT) vary greatly when considering
4 RFCs separately. For instance, the Lower Mississippi (LM) displays a good agreement
5 regardless of the dataset considered (Fig. 3b). PRISM (3.64 mm/day) presents the best
6 agreement with GHCN-D (3.75 mm/day). Little differences are found between 3B42 and
7 3B42RT in terms of average rain rate of 3.87 mm/day and 3.90 mm/day respectively with
8 however a narrower distribution (lower σ) for the bias-adjusted 3B42 than for 3B42RT.
9 Over the Missouri Basin River (MB), important differences are observed between 3B42
10 and 3B42RT with respect to GHCN-D. The bias-adjusted 3B42 displays a satisfying
11 agreement with surface observations that contrasts with the overestimation displayed by
12 the near real time 3B42RT observations (Fig. 3c). Over Northwest (NW), the bias-
13 adjusted 3B42 presents a substantial improvement when compared to 3B42RT but severe
14 underestimation remains for precipitation above 4 mm/day (Fig. 3d). Although closer to
15 surface observations, Stage IV displays a similar underestimation at higher rain rates.
16 Table 2 summarizes the differences between GHCN-D and the other datasets. For
17 PRISM, the linear regression coefficient when compared to surface observation (GHCN-
18 D) remains within a narrow range (0.97 to 1.03) for the different RFCs considered. The
19 differences are statistically significant at the 5% significance for about half of the RFCs
20 (5 over 12). For Stage IV, the variations are greater and indicate a general
21 underestimation with (a) varying between 0.87 and 1 and statistically significant
22 differences for 9 of the RFCs. The bias-adjusted 3B42 presents a wider variation range

1 (0.63 < a < 1.11), which is noticeably narrower than the coefficient obtained with the
2 near real time precipitation estimates 3B42RT (0.52 < a < 1.42).

3 Figure 4a displays the average annual precipitation derived from all datasets for
4 the different RFCs. The Lower Mississippi River Basin (LM) exhibits the higher average
5 annual rain rate regardless of the dataset. The Colorado Basin River (CB) displays the
6 lower average annual rain rate for GHCN-D, PRISM, Stage IV, and 3B42. For 3B42RT
7 the minimum is found for California Nevada (CN). The differences with respect to
8 GHCN-D are presented in Figure 4b. Over CONUS differences are found between -6.4%
9 (St. IV) and +6.1% (3B42RT). For PRISM differences are below 4% regardless of the
10 RFC considered. CONUS-wide, the precipitation estimates derived from 3B42 and
11 3B42RT are relatively close with a slightly lower rain rate for 3B42 (-4%). The
12 magnitude of the bias adjustment (difference between 3B42RT and 3B42) remains below
13 7% over most of the basins (AB: +5%, CN: -7%, LM: +0.7%, NW: -7%, OH: -3%, SE: -
14 3%, WG: +4%). This can be explained by the fact that 3B42RT uses an a-priori bias
15 adjustment based on climatological for the near real time algorithm (Huffman et al 2007,
16 Huffman and Bolvin 2013). Important bias correction is performed over the Midwest
17 (MB) with a +38% difference between 3B42RT and 3B42, reducing the differences with
18 GHCN-D from +49% down to +9% for 3B42RT and 3B42 respectively. This correction
19 is to account for the overestimation of summertime convection by Passive Microwave
20 retrieval that tends to associate important sub-cloud evaporation with precipitation as we
21 will see in the next section. The Colorado Basin (CB) RFC is the domain that displays
22 the most important difference between 3B42RT and 3B42 (+42%). For the remaining
23 RFCs, the differences between 3B42RT and 3B42 remains moderate between -21% and

1 +12% (MA: -17%, NC: +12%, NE: -21%). Stage IV presents globally lower differences
2 with GHCN-D (-14% to +1%) and PRISM (-17% to +4%) than the satellite estimates
3 3B42 (-28% to +7%) and 3B42RT (-32% to +49%). At the RFC level, Stage IV almost
4 systematically underestimates precipitation except for two RFCs (AB, MB) with a lower
5 rainfall of -7% when compared to GHCN-D CONUS-wide (Table 2). For the western
6 RFCs (CB, NW), Stage IV presents a better agreement with surface observations (-12%)
7 than 3B42 (-23%) and 3B42RT (-25%). The lower differences can be explained by the
8 fact that the western RFCs use the Mountain Mapper approach and gauge-only estimates
9 (Hou et al. 2014, Nelson et al. 2015).

10

11 **4. Seasonal precipitation**

12 4.1 – Seasonal precipitation patterns

13 Figure 5 displays the seasonal precipitation for winter (DJF: left) and summer
14 (JJA: right) for PRISM (Fig. 5a), Stage IV (Fig. 5b), 3B42 (Fig. 5c), and 3B42RT (Fig.
15 5d). PRISM and Stage IV present similar precipitation patterns regardless of the season.
16 By comparison with 3B42RT, the monthly-adjusted 3B42 displays precipitation patterns
17 visually closer to those of PRISM. The differences between 3B42RT and 3B42 are more
18 emphasized on a seasonal basis than observed for the annual basis (Fig. 2). For winter,
19 the bias-adjusted 3B42 precipitation estimates are lower than 3B42RT ($3B42 < 3B42RT$)
20 over the Rockies (CB), over the highest latitudes along the US/Canadian border (NC,
21 MB, NW), and East of the Mississippi (LM, SE). Conversely, the 3B42 estimates are
22 found higher than the near-real time 3B42RT ($3B42 > 3B42RT$) along the West coast from
23 Northern California up to the Pacific Northwest (NW, CN). For summer, the 3B42

1 estimates are found to be very significantly lower than 3B42RT (3B42<3B42RT) over
2 the Midwest (MB, NC, AB). The rain gauge adjustment performed retrospectively
3 corrects the possible overestimation of summertime convection by PMW sensors that
4 mistake sub-cloud evaporation for precipitation (Dinku et al. 2010, 2011, Ochoa et al.
5 2014). Similarly, for the area of the Lower Mississippi domain (LM) located East of the
6 Mississippi, 3B42 estimates are lower than 3B42RT.

7

8 4.2 – Comparison with surface observations

9 Figures 6a-b present the seasonal rain-rates derived from the different datasets.
10 Between the warm and cold season, average seasonal rain rate derived from surface
11 observations (GHCN-D, PRISM) vary from -95% for CN to +270% for MB (Table 3).
12 For winter, the minimum (maximum) average rain rate is found for MB (LM) with 0.64
13 mm/day (3.77 mm/day). For summer, the minimum (maximum) average rain rate is
14 found for CN (SE) with 0.17 mm/day (4.53 mm/day). We note that the seasonal minima
15 and maxima are observed for the same RFCs regardless of the dataset except for the
16 winter minimum for 3B42RT (Table 3). Seasonal differences between GHCN-D and
17 PRISM remain moderate (-5.9% to +2.1%) and comparable to that for the annual basis
18 (Fig. 6c-d). For stage IV, differences with GHCN-D vary from -18% to -2% (overall
19 underestimation) for winter and from -28% to +8% (overall underestimation) for summer.
20 For 3B42, the differences with GHCN-D range from -38% to +25% (no overall
21 under/overestimation) in winter. In addition to fundamental limitations in radar and
22 satellite measurement for snow and mixed precipitation events, additional uncertainties
23 are introduced from in-situ data that are used either in the adjustment (HADS, ASOS,

1 AWOS) or in the evaluation (GHCN-D) of remotely sensed products. Among the
2 systematic errors in measuring frozen precipitation, are evaporation, chimney effect,
3 wind field deformation, wetting losses, delayed tips due to snow melting in the funnel, or
4 uncertainties due to human intervention in the measurement procedure (Goodison et al.
5 1998, Groisman et al. 1999, Sevruk et al. 2009, Prat and Barros 2010b, McMillan et al.
6 2012, Leeper et al. 2015). Although, this point is beyond the scope of this study, we note
7 that the differences observed between remotely sensed and in-situ data for the higher
8 latitude RFCs (CB, MB, NC, NE, NW, OH) are within the range of that observed for the
9 other RFCs experiencing cold precipitation less frequently (-4.7% to -14.8% vs. -1.5% to
10 -18.0% for Stage IV and -31.1% to +16.7% vs. -38.0% to +16.7% for 3B42) (Table 3).
11 For summer, differences between 3B42 and GHCN-D present a narrower range from -2%
12 to +25% (overall overestimation). Those differences represent a substantial improvement
13 over those observed for the near real time 3B42RT, which vary from -49% to +147% in
14 winter and from -4% to +92% in summer (Table 3). The differences between 3B42RT
15 and 3B42 are the most important for MB and CR in winter (+111% and +58%
16 respectively), or CN and MB in summer (+54% and +49% respectively). The situations
17 where the highest differences are observed correspond to significant positive biases of
18 3B42RT (Table 3).

19 A closer insight into seasonal differences can be seen in Figure 7 that displays
20 scatterplots and Q-Q plots for the seasonal rain-rate over Northwest (NW). Regardless of
21 the season (winter: Fig. 7a; summer: Fig. 7b), PRISM presents a very good agreement
22 with surface observations with differences of 2-3% for the average rain-rate regardless of
23 the season. There is a four-fold difference between the maximum rain rates for winter (R

1 ≈ 12 mm/day) and summer ($R \approx 3$ mm/day). For winter, Stage IV displays a moderate
2 underestimation (-12%) when compared to GHCN-D. TMPA 3B42 presents a rainfall
3 distribution heavily skewed toward lower rain rates ($R < 6$ mm/day) when compared with
4 GHCN-D ($R > 12$ mm/day). Despite performing monthly-corrected accumulation for
5 3B42, a strong negative bias remains with a mean seasonal averaged rain rate about -30%
6 lower when compared to GHCN-D and PRISM. For rain rates greater than 4 mm/day,
7 the bias-adjusted 3B42 present a significant improvement when compared to the near real
8 time 3B42RT. However, a strong negative bias remains for 3B42 that displays a
9 comparable mean seasonal precipitation (≈ 2.5 mm/day) than 3B42RT, which is about -
10 30% when compared to surface observations. Summer exhibits average rain rates (≈ 0.82
11 mm/day) 4 times lower than winter (3.5 mm/day) (Fig. 7b). Stage IV displays a negative
12 bias for summer when compared to GHCN-D and PRISM ($\approx -19\%$) and comparable with
13 the bias observed for winter (-12%). Differences remain significant despite the fact that
14 Stage IV uses the PRISM/Mountain Mapper algorithm that combines automated rain
15 gauge observations and PRISM monthly precipitation climatology (Hou et al. 2014,
16 Nelson et al. 2015). Conversely, 3B42 presents a very good agreement with GHCN-D (-
17 1.7%) and PRISM (-2.4%) and contrasts with the severe underestimation observed on the
18 right side of the distribution during winter (Fig. 7a). The real-time 3B42RT displays
19 small biases when compared to GHCN-D (+2.4%) and PRISM (+0.4%). However, rather
20 than the indication of a good performance, results show that the locations with
21 overestimation are compensated by those with underestimations as can be seen with the
22 Q-Q plot aligning along the diagonal. A closer look indicates that the 3B42RT pixels
23 displaying the strongest underestimation ($< -50\%$) with respect to GHCN-D are located

1 West of the Cascades mountain range for low to moderate elevation (<500m) (not
2 shown). Comparatively, the pixels that display the strongest overestimation (>50%) are
3 found East of the Cascades regardless of the elevation. However, while the average rain
4 rate remains relatively constant East of the Cascades throughout the year ($R \approx 2\text{mm/day}$),
5 the seasonal differences are more important West of the Cascades with average rain rates
6 of less than 2mm/day in Summer to be compared with more than 5mm/day in Winter.
7 The important underestimation by 3B42RT West of the Cascades regardless of the
8 season, illustrates the difficulties for satellite to capture orographic and cold season
9 precipitation. We also note that despite the bias-adjustment, underestimation remains for
10 3B42 in winter due to uncertainties related to cold season precipitation measurements
11 mentioned earlier or by rain gauge locations that cannot fully capture orographic effects
12 that can be observed over distances smaller than the satellite resolution (Prat and Barros
13 2010a).

14 Further illustration of the importance of the bias-adjustment 3B42 can be found
15 in Figure 8 that displays comparisons over the Missouri Basin River (MB). Again,
16 GHCN-D and PRISM present an average rain rate difference of about 3% regardless of
17 the season. Similarly, Stage IV presents a good agreement with surface observations
18 with a small underestimation of -5% for winter (Fig. 8a) and a moderate overestimation
19 of +8.4% for summer (Fig. 8b). For both the cold and the warm season, the improvement
20 brought by the 3B42 bias-adjustment is clearly visible. For winter, the near real time
21 3B42RT exhibits a severe overestimation of +147% with respect to surface observation,
22 which is reduced to +16.7% for the bias-adjusted 3B42 (Table 3). A closer look at the
23 wintertime precipitation (Fig. 5d) indicates higher rainfall accumulation for 3B42RT at

1 higher latitudes and along the edges of the MB RFC when compared to the other datasets
2 (Fig. 5a-c). These differences are certainly associated with cold season precipitation and
3 are due to the challenge of measuring falling snow and frozen precipitation and
4 precipitation over snow and ice-covered areas by sensors (SSM/I, AMSU-B) used in the
5 near-real time 3B42RT (Huffman and Bolvin 2013). For summer, the bias-adjusted 3B42
6 exhibits moderate differences of +7.7% with respect to GHCN-D to be compared with an
7 overestimation of +61% for 3B42RT (Table 3). The overestimation of 3B42RT is found
8 consistently throughout the rain rate spectra (Fig. 8b). As mentioned earlier, the 3B42RT
9 overestimation is due to uncertainties in PMW retrievals that associate summertime sub-
10 cloud evaporation with precipitation (Dinku et al. 2010, 2011, Ochoa et al. 2014). The
11 monthly bias-adjustment (3B42) corrects efficiently for both the cold and warm season
12 3B42RT rainfall overestimation with a reduction of the average rain rate of about 110%
13 and 50% for winter and summer respectively. Overall, the bias-adjusted 3B42 performed
14 very well over the Great Plains (MB, NC) to correct for the overestimation of
15 summertime convection (Table 3) with comparable results than Stage IV (Table 3).
16 Important differences remained however for low daily rainfall (< 1mm/day) and for the
17 western RFCs during wintertime mostly due to the difficulty in capturing orographic
18 precipitation and uncertainties in retrieving cold precipitation by the satellite (Chen et al.
19 2013, Huffman and Bolvin 2013) but also and by the rain gauges used in the bias-
20 adjustment and the evaluation (Goodison et al. 1998, Groisman et al. 1999, Leeper et al.
21 2015)..

22

23 **5. Daily precipitation**

1 5.1 – Conditional analysis and extreme precipitation

2 After investigating the ability of the different datasets to describe precipitation
3 patterns, this section investigates their ability to capture intense and extreme precipitation
4 at the daily scale. A conditional analysis was conducted using different thresholds for
5 daily accumulation (Fig. 9). Figure 9a displays the average number of rainy days by year
6 derived from GHCN-D (first column), Stage IV (second column), 3B42 (third column),
7 and 3B42RT (fourth column). For Stage IV, TMPA 3B42, and TMPA 3B42RT the daily
8 accumulation is computed 12Z-12Z. For GHCN-D, the daily accumulation computed
9 depends on the local time and is 7:00LST-7:00LST for most of the locations, which
10 corresponds to 12Z-12Z on the Eastern US. Therefore, some uncertainties could arise
11 from computing daily accumulation over a slightly different time period. Although the
12 number of rainy days appears consistent in term of magnitude for the different
13 observation platforms, there are noticeable differences over specific areas. Despite a
14 delicate visual comparison between point data measurements from GHCN-D and Stage
15 IV gridded estimates due to the scarcity of station coverage, both products present a very
16 similar pattern and a comparable number of rainy days throughout CONUS. When
17 compared to Stage IV, 3B42 displays a lower number of rainy days over the Northeast
18 (NE), Middle-Atlantic (MA), and Ohio River Basin (OH). Similarly, a lower number of
19 rainy days are observed for 3B42 over the Northwest (NW) when compared to Stage IV.
20 On the other hand, 3B42 displays a higher number of rainy days over the Rockies
21 encompassing part or all of the Missouri Basin River (MB), Colorado Basin River (CB),
22 and California Nevada (CN) when compared to Stage IV. Different sensitivity for light
23 rainfall detection thresholds for each sensor, the ability to retrieve snow/frozen

1 precipitation, beam blockage over the Rockies, and/or the influence of temporal and
2 spatial resolution, can explain the differences. For instance, Stage IV higher spatial
3 resolution could improve the detection of localized events as compared to the satellite's
4 coarser resolution. Overall, the rain gauge adjusted radar (Stage IV) and satellite (3B42)
5 datasets display a satisfying visual agreement over CONUS despite the local differences
6 mentioned above. More important differences are observed with the real-time 3B42RT
7 dataset. Differences between the rain gauge adjusted satellite dataset 3B42 and 3B42RT
8 are particularly important over the Western US (Rocky Mountains) and at higher latitudes
9 with more rainy days for 3B42RT. For daily accumulation greater than the Wet
10 Millimeter Days (WMMD: $R > 17.8$ mm/day), significant differences are found over the
11 Northwest (NW) and over the Southeastern US (LM, SE) (Fig. 9b). The Wet Millimeter
12 Day threshold corresponds to the precipitation days that exceed the highest daily average
13 over the area considered (Shepherd et al. 2007). For North America, this maximum daily
14 average (17.8 mm/day) is recorded in Henderson Lake (British Columbia) (Source
15 NCDC). Both Stage IV and 3B42 display similar distribution patterns of WMMD. The
16 most important differences are found over the Northwest (NW). The differences between
17 GHCN-D and Stage IV are due to the scarcity of station coverage over the Pacific
18 Northwest Coast. For the gridded estimates, Stage IV displays a higher number of
19 WMMD when compared to bias-adjusted satellite estimates 3B42. The biggest
20 differences are observed with 3B42RT that shows a much lower number of rainy days
21 greater than WMMD (Fig. 9b). This is consistent with the underestimation observed for
22 the daily averages for 3B42RT and to a lesser extent for 3B42 (Fig. 3d, Fig. 7a-b). The
23 bias-adjustment increases the number of WMMD of 3B42 closer to Stage IV levels.

1 Conversely, 3B42 and 3B42RT that displayed less rainy days than Stage IV (Fig. 9a),
2 presents a higher occurrence of WMMD when compared to Stage IV over the Northeast
3 (NE), the upper part of the North Central (NC) domain, and the Lower Mississippi (LM)
4 (Fig. 9b). For daily accumulation greater than 2 in day^{-1} ($> 50.8 \text{ mm/day}$: Karl and
5 Plummer 1995; hereafter EPD2), GHCN-D and Stage IV display comparable counts for
6 EPD2 over the Eastern US where rain gauges coverage is denser (Fig. 9c). Over the
7 Northeast (NE) and the Southeastern US (LM, SE), 3B42 and 3B42RT display a higher
8 number of days with rainfall above 2 in day^{-1} as compared to Stage IV. Daily
9 precipitation greater than 4 in day^{-1} ($> 101.6 \text{ mm/day}$: Barlow 2011; hereafter EPD4) is
10 limited to the Pacific Coast and East of 100°W , a domain regularly impacted by tropical
11 cyclones (Prat and Nelson 2013a,b, 2014a) (Fig. 9d). These EPD4 events are relatively
12 infrequent (3 counts or less by year) and roughly correspond to the 0.1-0.5% top daily
13 events regardless of the RFC considered. The bias-adjusted 3B42 and real-time 3B42RT
14 display a comparable number of EPD4 events over the Southeastern US. The maximum
15 occurrences are observed over the Lower Mississippi (LM) RFC and are higher than the
16 daily counts for Stage IV. Over the Northwest, the bias-adjusted (3B42) is able to better
17 capture those extreme daily accumulation events (EPD4) with respect to 3B42RT that
18 displays almost no days with rainfall above 4 in day^{-1} .

19 More quantitative information can be found in Figure 10 that displays the
20 proportion of rain gauges (GHCN-D) and the corresponding radar (Stage IV) or satellite
21 (3B42, 3B42RT) pixels experiencing the different daily accumulation thresholds
22 (WMMD, EPD2, EPD4) over the 11-year period. For CONUS (central panel), we note
23 that this proportion of stations/pixels experiencing WMMD, EPD2, and EPD4 are

1 comparable regardless of the platform considered. For instance, all stations/pixels
2 experience WMMD during the 11-year period (100%). For EPD2, the ratio remains
3 relatively close regardless of the sensor and varies from 88% (Stage IV) to 95%
4 (3B42RT). Similarly for EPD4, the proportion is about 60% (GHCN, 3B42, 3B42RT)
5 with a slightly lower ratio (54%) for Stage IV. Some interesting facts can be derived
6 from the isolated RFC figures (border figures). A few RFCs (AB, LM, MA, SE, WG)
7 display comparable ratios regardless of the sensor and the daily accumulation considered.
8 Apart from a couple of RFCs (NC, OH), the ratio of Stage IV pixels experiencing
9 extreme precipitation (EPD4) is relatively close to the ratio of GHCN. When looking at
10 satellite pixels, we observe a relative symmetry for the ratio of stations experiencing
11 EPD2. However, for Western (CN, NW) and Northeast (NE) RFCs we note a strong
12 asymmetry in the ratio of 3B42RT pixels experiencing extreme precipitation (EPD4)
13 when compared to the other sensors. This confirms the fact that over the Western US, the
14 non-adjusted satellite QPE severely underestimates extreme daily precipitation.
15 Interestingly, over the neighboring Colorado Basin River RFC (CB) we note a higher
16 proportion of 3B42RT pixels displaying EPD2 and EPD4 than observed for the other
17 sensors (GHCN, Stage IV, 3B42). Furthermore, regardless of the RFC and daily
18 accumulation considered, the ratio of pixels for 3B42 is very close to that of the GHCN
19 stations, hence providing confidence in the bias-adjustment performed. However those
20 results have to be interpreted with caution as they present a count of the daily events over
21 the 11-year period. The number of events decreases with increasing rain rate and the
22 WMMD correspond roughly to the 90th percentile precipitation events regardless of the
23 RFC (Nelson et al. 2015). A test was performed to determine the interstation correlation

1 of daily precipitation events corresponding to the 90th percentile (not shown). For each
2 station, the correlation was computed using the daily events greater than the 90th
3 percentile regardless of the values of the other stations. Results showed that for those
4 high-intensity events, the average correlation distance was about 30-80-km which is
5 comparable with the satellite footprint.

6 Figure 11 provides a count of the total number of rainy days (Fig. 11a), WMMD
7 (Fig. 11b), EPD2 (Fig. 11c), and EPD4 (Fig. 11d) for GHCN-D, Stage IV, 3B42, and
8 3B42RT over CONUS and for each RFC at the rain gauge location. For the number of
9 rainy days, we note that 3B42 and 3B42RT provide comparable results and display less
10 variability across the RFCs when compared to GHCN-D and Stage IV. For GHCN and
11 Stage IV, the RFCs over the Rockies or located partially West of 95°W (AB, CB, CN,
12 WG) display about half of the rainy days than the Eastern (MA, NC, NE, OH, SE) and
13 Northwest (NE) RFCs. The Colorado Basin (CB) presents consistently the lowest
14 average number of events by active stations regardless of the daily accumulation
15 (WMMD, EPD2, EPD4). On the other hand, the Lower Mississippi (LM) present the
16 highest average number of events regardless of the sensor considered. For selected
17 RFCs, the differences between 3B42 and 3B42RT are particularly important for EPD2
18 and EPD4. The biggest differences are found for Northwest (NW) and the Missouri
19 Basin River (MB). For the latest, the number of EPD2 and EPD4 events for 3B42RT is
20 about 50% and 130% higher respectively than for 3B42 and is attributed to summertime
21 convection and sub-cloud evaporation over the Midwest mentioned earlier. Over NW,
22 the number of EPD2 and EPD4 events retrieved after bias-adjustment (3B42) is 6- and 3-
23 fold the number of events indicated by 3B42RT due to the difficulty of capturing extreme

1 precipitation in real-time over the area. For the latest case, consider that those events
2 (EPD4) correspond to only a handful of occurrences for the period 2002-2012, and
3 caution is necessary when analyzing those results.

4

5 5.2 – Contingency analysis between Stage IV and GHCN-D

6 The previous results were provided for the entire period 2002-2012. Figure 12
7 displays a contingency analysis between daily precipitation from the GHCN-D stations
8 and the corresponding Stage IV radar pixel. We will assume that the rain gauge is
9 representative of the grid-averaged rainfall for Stage IV. The computation of the
10 interstation correlation for daily events indicated that the correlation distance was greater
11 than the 4-km spatial resolution of the radar (not shown). The number of rainy days ($R >$
12 0 mm/day) observed simultaneously at the rain gauge and the radar pixel is 62% over
13 CONUS (Fig. 12a). Significant differences are observed between RFCs and vary from
14 49% (CB) to 71% (OH). Events observed only by the radar are 24% over CONUS,
15 which is higher than the ratio for gauge only events (14%). A similar trend is observed
16 regardless of the RFC considered ranging from 18% (NE) to 32% (MB) for events at the
17 radar pixel only and from 8% (AB) to 22% (CN) for rain gauge only events. With
18 increasing rain rate the number of events observed simultaneously by the gauge and the
19 radar decreased from 62% ($R > 0$ mm/day: Fig. 2a), to 56% (WMMD: Fig. 12b), to 43%
20 (EPD2: Fig. 12c), and to 35% (EPD4: Fig. 12d). Furthermore, while the ratio of events
21 observed at the radar pixel only remain relatively close around 20% regardless of the
22 daily rainfall threshold (i.e. between 17% for WMMD and 24% for $R > 0$ mm/day), the
23 number of events missed by the radar increases from 14% ($R > 0$ mm/day) to 45%

1 (EPD4). In addition for accumulation greater than 2 in day^{-1} , the number of extreme
2 events missed by one or the other sensor is greater than the number of events observed
3 simultaneously by both sensors (Fig. 12c). For accumulation greater than 4 in day^{-1} , the
4 proportion of events missed by the radar becomes more important except for the
5 Arkansas-Red Basin (AB) RFC.

6 Figure 13 displays the contingency analysis at each station location. Regardless of
7 the daily accumulation ($R > 0 \text{ mm/day}$: Fig. 13a), the Eastern US and West Coast stations
8 present a higher proportion of events observed simultaneously at the rain gauge and radar
9 pixel (median column). There is a strong contrast between the he Eastern and Western
10 US with the Eastern US displaying a lower proportion of events observed at the gauge
11 only. With increasing daily accumulation (Fig. 13b-d), the number of rainfall events
12 decreases over the Rockies, the Western and Northern US as described previously (Fig.
13 8). While the spatial extent of intense precipitation events becomes more and more
14 limited to the Southeastern US with increasing daily accumulation, the ratio of events
15 observed at the radar pixel only (right column) remains relatively constant. For
16 concurrent rainfall events (median column) the ratio decreases significantly for daily
17 accumulation greater than 2 in day^{-1} (Fig. 13c). With increasing daily accumulation, as
18 the number of events become smaller and spatially more localized, the ratio of events
19 missed by the radar increases importantly over Midwest (Fig. 13b-d). However, caution
20 is advised when looking at increasing threshold events in particular over areas where
21 those events become more and more scarce. A closer look shows that most of the events
22 observed at one or the other sensor (NY: left column; YN: right column) for
23 accumulation greater than EPD2 and EPD4 are single occurrence events. For EPD2, the

1 single occurrence events are located West of the -103°W longitude (Fig. 13e). For EPD4,
2 apart from isolated events over the Rockies and the Pacific coast, most of single
3 occurrence events are located at the edge of the Southeastern US, i.e. East of -100°W and
4 North of the 40°N latitude (Fig. 13f).

5

6 **6. Summary and Conclusion**

7 We compared quantitative precipitation estimates from satellite (3B42 and
8 3B42RT) and radar (Stage IV) with surface observations (GHCN-D) and models
9 (PRISM) over CONUS for the period 2002-2012. The comparisons were performed at
10 the annual, seasonal, and daily scales over the major river basins within CONUS. The
11 main conclusions of this study are summarized below.

- 12 • Over CONUS the different datasets show a satisfying agreement on an annual basis
13 with differences ranging between -6.4% (St. IV) and $+6.1\%$ (3B42RT). At the RFC
14 level, PRISM displays a difference of $\pm 4\%$ with GHCN-D. Stage IV presents a
15 tendency to underestimate when compared to surface observations (-14% to $+1\%$). A
16 bigger spread of the differences is found between 3B42 and GHCN-D (-28% to
17 $+9\%$). Finally, 3B42RT displays the bigger differences with GHCN-D (-33% to
18 $+49\%$).
- 19 • The bias-adjusted 3B42 represents a significant improvement when compared to the
20 near real time 3B42RT. The 3B42RT biases were particularly important at the
21 seasonal scale over Northwest and the Western US (CN, NW) and at higher latitude
22 over the Midwest (MB, NC) during winter with an important underestimation (-35%)
23 of the daily accumulation in the first case (CN, NW), and a severe overestimation

1 (+100%) in the second case (MB, NC). During summer, 3B42RT presents large
2 positive biases (+45%) over the Midwest (MB, NC). The bias adjustment (3B42)
3 reduces those differences to moderate levels (i.e. from +100% to +22% in winter and
4 from +45% to +7% in summer). Over the CNRFC, 3B42RT presents alternatively a
5 severe underestimation for winter (-45%) and a severe overestimation for summer
6 (+121%) with an overall annual differences of -23% with surface observations
7 GHCN-D.

8 • Despite the bias-adjustment, large biases remained for 3B42 at higher daily average
9 accumulation (> 5 mm/day) over CONUS. Discrepancies can be explained by the
10 difference between point (RG) and area (satellite, radar) measurements and the
11 difficulty in capturing localized, convective, and orographic events due to the coarser
12 resolution. Furthermore, those differences can be more important at the seasonal
13 scale and for selected basins in particular over the Western part of CONUS (Pacific
14 Northwest, Rocky Mountains) due to the difficulty in retrieving precipitation over
15 mountainous areas.

16 • Stage IV presents an overall better agreement with surface observations than 3B42.
17 At the seasonal level Stage IV displays the same tendency of rainfall underestimation
18 with respect to surface observations with differences ranging from -18% to -2% for
19 winter and from -28% to +8% for summer. Comparatively, 3B42 displays a bigger
20 spread with no particular tendency (-38% +25%) for winter and a tendency of rainfall
21 overestimation (-2% to +25%) for summer.

22 • At the daily scale, the conditional analysis performed using increasing daily
23 precipitation thresholds (0-4 in day^{-1}), showed that the sensor ability to capture

1 intense and extreme precipitation depended on the domain considered. In particular,
2 the near real time satellite QPE 3B42RT displayed poor skills in capturing intense
3 daily precipitation over the Northwest. The bias-adjusted 3B42 exhibited a
4 significant improvement and level closer to surface station (GHCN-D) and radar
5 statistics (Stage IV) over the 11-year period.

- 6 • A contingency analysis performed at the rain gauge location and the corresponding
7 radar pixel, showed that with increasing daily accumulation from greater than 0 to
8 greater than 4 in day^{-1} , the ratio of events observed simultaneously by the gauge and
9 the radar decreased from 62% to 45%. Furthermore, while the ratio of events
10 observed only by the radar remained close (around 20%) regardless of the daily
11 accumulation, the number of events measured at the ground but missed by the radar
12 increased from 15% to 45%. Although caution is required due to the fact that large
13 rainfall events above 2 in day^{-1} (a fortiori events greater than 4 in day^{-1}) are infrequent
14 and geographically limited to the Pacific Northwest and the Eastern US, results
15 illustrate the challenge of retrieving extreme precipitation (top 1% percentile) from
16 remote sensing.

1 **Acknowledgement**

2 This research was supported by the NOAA/NCDC Climate Data Records and Science
3 Stewardship Program through the Cooperative Institute for Climate and Satellites - North
4 Carolina under the agreement NA09NES4400006.

1 **References**

- 2 Ashouri, H, Hsu, K., Sorooshian, S., Braithwaite, D., Knapp, K. R., Cecil, L. D., Nelson,
3 B. R., and Prat, O. P.: PERSIANN-CDR: Daily precipitation climate data record from
4 multi-satellite observations for hydrological and climate studies. Bull. Am. Meteorol.
5 Soc., in press, 2015.
- 6 Barlow, M.: Influence of hurricane-related activity on North American extreme
7 precipitation. Geophys. Res. Lett. 38, L04705, doi:10.1029/2010GL046258, 2011.
- 8 Ciach, G. J., Habib, E., and Krajewski, W. F.: Zero-covariance hypothesis in the error
9 variance separation method of radar rainfall verification. Adv. Water Resour., 26,
10 573-580, 2003.
- 11 Ciach, G. J., and Krajewski, W. F.: On the estimation of rainfall error variance. Adv.
12 Water Resour., 2, 585-595, 1999.
- 13 Ciach, G. J., Krajewski, W. F., and Villarini, G.: Product-error-driven uncertainty model
14 for probabilistic quantitative precipitation estimation with NEXRAD data. J.
15 Hydrometeorol. 8, 1325-1347, 2007.
- 16 Chen, S., Hong, Y., Gourley, J. J., Huffman, G. J., Tian, Y., Cao, Q., Yong, B., Kirstetter,
17 P.-E., Hu, J., Hardy, J., Li, Z., Khan, S. I., and Xue, X.: Evaluation of the successive
18 V6 and V7 TRMM multisatellite precipitation analysis over the Continental United
19 States, Water Resour. Res., 49, 8174–8186, doi:10.1002/2012WR012795, 2013.
- 20 Chen, M., Xie, P., Janowiak, J. E., and Arkin, P. A.: Global land precipitation: a 50-yr
21 monthly analysis based on gauge observations. J. Hydrometeorol., 3, 249-266, 2002.

- 1 Daly, C., Neilson, R. P., and Phillips, D. L.: A statistical-topographic model for mapping
2 climatological precipitation over mountainous terrain. *J. Appl. Meteor.*, 33, 140-158,
3 1994.
- 4 Dinku, T., Ruiz, F., Connor, S. J., and Ceccato, P.: Validation and Intercomparison of
5 Satellite Rainfall Estimates over Colombia, *J. Appl. Meteorol. Climatol.*, 49, 1004-
6 1014, doi:10.1175/2009JAMC2260.1, 2010.
- 7 Dinku, T., Ceccato, P., and Connor, S. J.: Challenges of satellite rainfall estimation over
8 mountainous and arid parts of east Africa, *Int. J. Remote Sens.*, 30, 5965-5979,
9 doi:10.1080/01431161.2010.499381, 2011.
- 10 Goodison, B. E., Louie, P. Y. T., and Yang, D.: WMO solid precipitation measurement
11 intercomparison. WMO Instruments and Observing Methods Rep., WMO/TD-872,
12 212 pp., 1998.
- 13 Groisman, P. Y., Peck, E. L., and Quayle, R. G.: Intercomparison of Recording and
14 Standard Nonrecording U.S. Gauges , *J. Atmos. Ocean. Tech.*, 16, 602-609, 1999.
- 15 Gutowski Jr., W. J., Decker, S. G., Donavon, R. A., Pan, Z., Arritt, R. W, and Takle E.
16 S.: Temporal–Spatial Scales of Observed and Simulated Precipitation in Central U.S.
17 Climate. *J. Climate*, 16, 3841-3847, 2003.
- 18 Habib, E., Ciach, G. J, and Krajewski, W. F.: A method for filtering out raingauge
19 representativeness errors from the verification distributions of radar and raingauge
20 rainfall. *Adv. Water Resour.*, 27, 967-980, 2004.
- 21 Hou, D., Charles, M., Luo, Y., Toth, Z., Zhu, Y., Krzysztofowicz, R., Lin, Y., Xie, P.,
22 Seo, D.-J., Pena, M., and Cui, B.: Climatology-Calibrated Precipitation Analysis at

1 Fine Scales: Statistical Adjustment of Stage IV toward CPC Gauge-Based Analysis.
2 J. Hydrometeorol., 15, 2542-2557, 2014.

3 Huffman, G. J., Adler, R. F., Bolvin, D. T. Gu, G., Nelkin, E. J., Bowman, K., Hong, Y.,
4 Stocker, E. F., and Wolf, D. B.: The TRMM multisatellite precipitation analysis
5 (TMPA): Quasi-global, multiyear, combined-sensor precipitation estimates at fine
6 scales. J. Hydrometeorol., 8, 38-55, 2007.

7 Huffman, G. J., Adler, R. F., Morrissey, M., Bolvin, D., Curtis, S., Joyce, R., McGavock,
8 B., and Susskind, J.: Global precipitation at one-degree daily resolution from multi-
9 satellite observations, J. Hydrometeorol., 2, 36-50, 2001.

10 Huffman, G. J., and Bolvin, D. T.: TRMM and Other Data Precipitation Data Set
11 Documentation, Lab. for Atmos., NASA Goddard Space Flight Cent. and Sci. Syst.
12 and Appl. Inc., Available at:
13 ftp://precip.gsfc.nasa.gov/pub/trmmdocs/3B42_3B43_doc.pdf (last access 28 Jan.
14 2015), 2013.

15 Joyce, R., Janowiak, J., Arkin, P., and Xie, X.: CMORPH: A method that produces global
16 precipitation estimates from passive microwave and infrared data at high spatial and
17 temporal resolution. J. Hydrometeorol., 5, 487-503, 2004.

18 Karl, T. R., and Plummer, N.: Trends in high-frequency climate variability in the
19 twentieth century. Nature, 377, 217-220, 1995.

20 Kidd, C., Levizzani, V., and Laviola, S.: Quantitative precipitation estimation from earth
21 observation satellites. Rainfall: State of the Science, Geophys. Monogr. Ser.
22 <http://dx.doi.org/10.1029/2009GM000920>, online first, 2010.

1 Kidd, C., Bauer, P., Turk, J., Huffman, G. J., Joyce, R., Hsu, K.-L., and Braithwaite, D.:
2 Intercomparison of high-resolution precipitation products over Northwest Europe. *J.*
3 *Hydrometeorol.*, 13, 67-83, 2012.

4 Leeper, R. D., Rennie, J., and Palecki, M. A.: Observational Perspectives from U.S.
5 Climate Reference Network (USCRN) and Cooperative Observer Program (COOP)
6 Network: Temperature and Precipitation Comparison, *J. Atmos. Ocean. Tech.*, in
7 press, 2015.

8 Lin, Y., and Mitchell, K. E.: The NCEP stage II/IV hourly precipitation analyses:
9 Development and applications. Preprints, 19th Conf. on Hydrology, San Diego, CA,
10 *Amer. Meteor. Soc.*, 9-13 January, Paper 1.2., 2005.

11 Liu, C., and Zipser, E. J.: Diurnal cycles of precipitation, clouds, and lightning in the
12 tropics from 9 years of TRMM observations. *Geophys. Res. Lett.*, 35, L04819,
13 doi:10.1029/2007GL032437, 2008

14 McMillan, H., Krueger, T., and Freer, J.: Benchmarking observational uncertainties for
15 hydrology: rainfall, river discharge, and water quality, *Hydrol. Process.*, 26, 4078-
16 4111, 2012.

17 Menne, M. J., Durre, I., Vose, R. S., Gleason, B. E., and Houston, T. G.: An overview of
18 the global historical climatology network-daily database. *J. Atmos. Oceanic Technol.*,
19 29, 897-910, 2012.

20 Michaelides, S., Levizzani, V., Anagnostou, E., Bauer, P., Kasparis, T., and Lane, J. E.:
21 Precipitation: measurement, remote sensing, climatology and modeling. *Atmos. Res.*,
22 94, 512-533, 2009.

1 Nelson, B. R., Prat, O. P., Seo, D.-J., and Habib, E.: Assessment and implications of
2 NCEP Stage IV quantitative precipitation estimates. *Wea. Forecast.* Under revision,
3 2015.

4 Nelson, B. R., Kim, D., and Seo, D.-J.: Multisensor precipitation reanalysis. *J.*
5 *Hydrometeorol.*, 11, 666-682, 2010.

6 Nesbitt, S. W., and Anders, A. M.: Very high-resolution precipitation climatologies from
7 the Tropical Rainfall Measuring Mission precipitation radar. *Geophys. Res., Lett.* 36,
8 L15815, doi:10.1029/2009GL038026, 2009.

9 Nesbitt, S. W., and Zipser, E. D.: The diurnal cycle of rainfall and convective intensity
10 according to three years of TRMM measurements, *J. Climate*, 16, 1456-1475, 2003.

11 Ochoa, A., Pineda, L., Crespo, P., and Willems, P.: Evaluation of TRMM 3B42
12 precipitation estimates and WRF retrospective precipitation simulation over the
13 Pacific–Andean region of Ecuador and Peru. *Hydrol. Earth Syst. Sci.*, 18, 3179–3193,
14 2014.

15 Prat, O. P., and Barros, A. P.: Assessing satellite-based precipitation estimates in the
16 Southern Appalachian Mountains using rain gauges and TRMM PR. *Adv. Geosci.*,
17 25, 143-153, 2010a.

18 Prat, O. P., and Barros, A. P.: Ground observations to characterize the spatial gradients
19 and vertical structure of orographic precipitation - Experiments in the inner region of
20 the Great Smoky Mountains, *J. Hydrol.*, 391, 143-158, doi:
21 10.1016/j.jhydrol.2010.07.013, 2010b.

22

1 Prat, O. P., and Nelson, B. R.: Precipitation contribution of tropical cyclones in the
2 Southeastern United States from 1998 to 2009 using TRMM precipitation data. *J.*
3 *Climate*, 26, 1047-1062, 2013a.

4 Prat, O. P., and Nelson, B. R.: Mapping the world's tropical cyclone rainfall contribution
5 over land using the TRMM Multi-satellite Precipitation Analysis. *Water Resour. Res.*
6 49, 7236-7254, doi:10.1002/wrcr.20527, 2013b.

7 Prat, O. P., and Nelson, B. R.: Characteristics of annual, seasonal, and diurnal
8 precipitation in the Southeastern United States derived from long-term remotely
9 sensed data. *Atmos. Res.*, 144, 4-20, 2014.

10 PRISM Technical Note: Descriptions of PRISM Spatial Climate Datasets for the
11 Conterminous United States. Tech. Note, 14 pp., <http://www.prism.oregonstate.edu/>,
12 last access: 1 October 2014, 2013.

13 Reed, S., and Maidment, D.: A GIS procedure for merging NEXRAD precipitation data
14 and digital elevation models to determine rainfall-runoff modeling parameters. Online
15 Report 95-3, Center for Research in Water Resources (CRWR), University of Texas
16 at Austin, 1995.

17 Reed, S., and Maidment, D.: Coordinate transformations for using NEXRAD data in
18 GIS-based hydrologic modeling. *J. Hydrol. Eng.*, 4, 174-182, 1999.

19 Sahany, S., Venugopal, V., and Nanjundiah, R.: Diurnal-scale signatures of monsoon
20 rainfall over the Indian region from TRMM satellite observations. *J. Geophys. Res.*,
21 115, D02103. <http://dx.doi.org/10.1029/2009JD012644>, 2010.

1 Sapiano, M. R. P., and Arkin, P. A.: An intercomparison and validation of high-
2 resolution satellite precipitation estimates with 3-hourly gauge data. *J.*
3 *Hydrometeorol.*, 10, 149–166, 2009.

4 Schneider, U., Becker, A., Finger, P., Meyer-Christoffer,, A., Rudolf, B., and Ziese, M.:
5 GPCP Monitoring Product: Near Real-Time Monthly Land-Surface Precipitation
6 from Rain-Gauges based on SYNOP and CLIMAT data. DOI:
7 10.5676/DWD_GPCP/MP_M_V4_100;
8 http://dx.doi.org/10.5676/DWD_GPCP/MP_M_V4_100, 2011.

9 Schneider, U., Becker, A., Meyer-Christoffer, A., Ziese, M., and Rudolf, B.: Global
10 Precipitation Analysis Products of the GPCP. Global Precipitation Climatology
11 Centre, DWD, 12 pp., available at [ftp://ftp-](ftp://ftp-anon.dwd.de/pub/data/gpcp/PDF/GPCP_intro_products_2008.pdf)
12 [anon.dwd.de/pub/data/gpcp/PDF/GPCP_intro_products_2008.pdf](ftp://ftp-anon.dwd.de/pub/data/gpcp/PDF/GPCP_intro_products_2008.pdf), last access 28
13 January 2015, 2010.

14 Shepherd, J. M., Grundstein, A., and Mote, T. L.: Quantifying the contribution of tropical
15 cyclones to extreme rainfall along the coastal southeastern United States, *Geophys.*
16 *Res. Lett.*, 34, L23810, doi:10.1029/2007GL031694, 2007.

17 Sorooshian, S., Hsu, K., Gao, X., Gupta, H., Imam, B., and Braithwaite, D.: Evolution of
18 the PERSIANN system satellite-based estimates of tropical rainfall. *Bull. Am.*
19 *Meteorol. Soc.*, 81, 2035-2046, 2000.

20 Sevruk, B., Ondras, M., and Chvila, B.: The WMO precipitation measurement
21 intercomparison, *Atmos. Res.*, 192, 376-380, 2009.

22 Tapiador, F. J., Turk, F. J., Petersen, W., Hou, A. Y., García-Ortega, E., Machado, L. A.
23 T., Angelis, C. F., Salio, P., Kidd, C., Huffman, G. J., and de Castro, M.: Global

1 precipitation measurement: methods, datasets and applications. *Atmos. Res.*, 104-105,
2 70-97, 2012.

3 Zhang, J., Howard, K., Langston, C., Vasiloff, S., Arthur, A., Van Cooten, S., Kelleher,
4 K., Kitzmiller, D., Ding, F., Seo, D.-J., Wells, E., and Dempsey, C.: National mosaic
5 and multi-sensor QPE (NMQ) system. *Bull. Am. Meteorol. Soc.*, 92, 1321-1338,
6 2011.

1 **LIST OF TABLES**

2 Table 1: List of the 12 NWS RFCs and corresponding number of GHCN-D rain gauges.

3

4 Table 2: Average rain rate (mm/day), and comparisons with surface observations
5 (GHCN-D) for annual precipitation estimated derived from PRISM, Stage IV, 3B42, and
6 3B42RT. The comparison [%|a|R²] includes the differences (%), and the linear
7 regression coefficients (a; R²) over CONUS and each RFC. For each QPE datasets, the
8 numbers in bold and italic-bold indicate the upper and lower limits when compared to
9 GHCN-D.

10

11 Table 3: Average rain rate (mm/day) and differences [%] between GHCN-D and other
12 annual precipitation estimates (PRISM, Stage IV, 3B42, 3B42RT) over CONUS and over
13 each RFC for winter (DJF) and summer (JJA). For each QPE datasets and season, the
14 numbers in bold and italic-bold indicate the upper and lower limits when compared to
15 GHCN-D.

16

17 **LIST OF FIGURES**

18 Figure 1: a) Locations of the GHCN-D rain gauges locations over CONUS: a) Total 8815
19 rain gauges, and b) The 4075 rain gauges reporting at least 90% of the time during the
20 period 2002-2012. c) National Weather Service (NWS) 12 River Forecast Centers
21 (RFCs).

22

1 Figure 2: Annual average precipitation derived from: a) PRISM, b) Stage IV, c) TMPA
2 3B42, and d) TMPA 3B42RT for the period 2002-2012.

3

4 Figure 3: Scatterplots (black) and Quantile-Quantile (red) plots for annual precipitation
5 derived from PRISM, Stage IV, TMPA 3B42, and TMPA 3B42RT when compared to
6 GHCN-D network for: a) CONUS, b) Lower Mississippi River Basin (LM), c)
7 Missouri Basin River (MB), and d) Northwest (NW) for the period 2002-2012. Please
8 note that for row c), the scale is different then for rows a), b), and d).

9

10 Figure 4: Average annual precipitation derived from GHCN-D, PRISM, Stage IV, TMPA
11 3B42, and TMPA 3B42RT for the different RFCs. Differences (%) with respect to
12 GHCN-D surface measurements.

13

14 Figure 5: Winter (DJF: Left Column) and summer (JJA: Right Column) precipitation
15 derived from: a) PRISM, b) Stage IV, c) TMPA 3B42, and d) TMPA 3B42RT for the
16 period 2002-2012.

17

18 Figure 6: Seasonal rain-rate derived from GHCN-D, PRISM, Stage IV, TMPA 3B42, and
19 TMPA 3B42RT for each RFC and for: a) Winter (DJF), and b) Summer (JJA).
20 Differences between GHCN-D and PRISM, Stage IV, TMPA 3B42, and TMPA 3B42RT
21 for: c) Winter (DJF), and d) Summer (JJA).

22

1 Figure 7: Scatterplots (black) and Q-Q plots (red) for the seasonal rain-rate for PRISM,
2 Stage IV, TMPA 3B42, and TMPA 3B42RT for: a) Winter (DJF), and b) Summer (JJA)
3 over Northwest (NW).

4

5 Figure 8: Scatterplots (black) and Q-Q plots (red) for the seasonal rain-rate for PRISM,
6 Stage IV, TMPA 3B42, and TMPA 3B42RT for: a) Winter (DJF), and b) Summer (JJA)
7 over Missouri Basin River (MB).

8

9 Figure 9: a) Number of rainy days ($RR > 0$ mm/day), b) Wet Millimeter Days (WMMD),
10 c) Extreme Precipitation Days greater than 2 in day^{-1} ($RR > 50.8$ mm/day: EPD2), and d)
11 Extreme Precipitation Days greater than 4 in day^{-1} ($RR > 101.6$ mm/day: EPD4) for Stage
12 IV and TMPA 3B42.

13

14 Figure 10: Proportion (%) of stations (GHCN-D) and corresponding pixel (Stage IV,
15 TMPA 3B42, TMPA 3B42RT) experiencing WMMD, EPD2, and EPD4 over CONUS
16 (central figure) and for the 12 River Forecast Centers (border figures).

17

18 Figure 11: Average number of: a) Rainy days, b) Wet Millimeter Days (WMMD) i.e.
19 precipitation days with accumulation greater than 17.8 mm/day, c) Precipitation Days
20 with accumulation greater than 2 in day^{-1} (EPD2), and d) Precipitation Days with
21 accumulation greater than 4 in day^{-1} (EPD4) for GHCN-D, Stage IV, TMPA 3B42, and
22 TMPA 3B42RT over CONUS and for the 12 River Forecast Centers (RFCs). Data are

1 for the period 2002-2012. The average number of days is normalized by the number of
2 locations experiencing at least one event (Fig. 10).

3

4 Figure 12: Contingency as a function of the daily threshold selected: a) $RR > 0$, b)
5 $RR > WMMD$, c) $RR > EPD2$, and d) $RR > EPD4$ for rainfall observed simultaneously at the
6 rain gauge and at the radar pixel [YY: red], and successively at the rain gauge only [YN:
7 blue], or at the radar pixel only [NY: green] over CONUS (circle) and for the 12 RFCs
8 (bars). Data are for the period 2002-2012.

9

10 Figure 13: Contingency analysis at the rain gauge site with respect to the daily rainfall
11 accumulation: a) $RR > 0$, b) $RR > WMMD$, c) $RR > EPD2$, and d) $RR > EPD4$ for rain
12 observed at the radar pixel only (first column), simultaneously at the rain gauge and radar
13 (second column), and at the rain gauge only (third column). e) and f) Same as c) and d)
14 but only displaying single event occurrence over the period 2002-2012.

1 Table 1: List of the 12 NWS RFCs and corresponding number of GHCN-D rain gauges.

Nbr	ID	Name	Number of COOP RG	
			Unconditional (Reporting 90% of time)	Unconditional (Total operational)
0	CONUS	CONUS	4075	8815
1	ABRFC	Arkansas Red Basin	325	637
2	CBRFC	Colorado Basin River	243	521
3	CNRFC	California Nevada	202	537
4	LMRFC	Lower Mississippi	363	728
5	MARFC	Middle Atlantic	166	378
6	MBRFC	Missouri Basin River	654	1385
7	NCRFC	North Central	541	1225
8	NERFC	Northeast	195	462
9	NWRFC	Northwest	260	570
10	OHRFC	Ohio River Basin	378	833
11	SERFC	Southeast	387	781
12	WGRFC	West Gulf	361	758

2

1 Table 2: Average rain rate (mm/day), and comparisons with surface observations (GHCN-D) for
2 annual precipitation estimated derived from PRISM, Stage IV, 3B42, and 3B42RT. The
3 comparison [%|a|R²] includes the differences (%), and the linear regression coefficients (a; R²)
4 over CONUS and each RFC. For each QPE datasets, the numbers in bold and italic-bold indicate
5 the upper and lower limits when compared to GHCN-D. The asterisk indicates that the datasets
6 are statistically different at the 5% significance level with respect to surface observations.

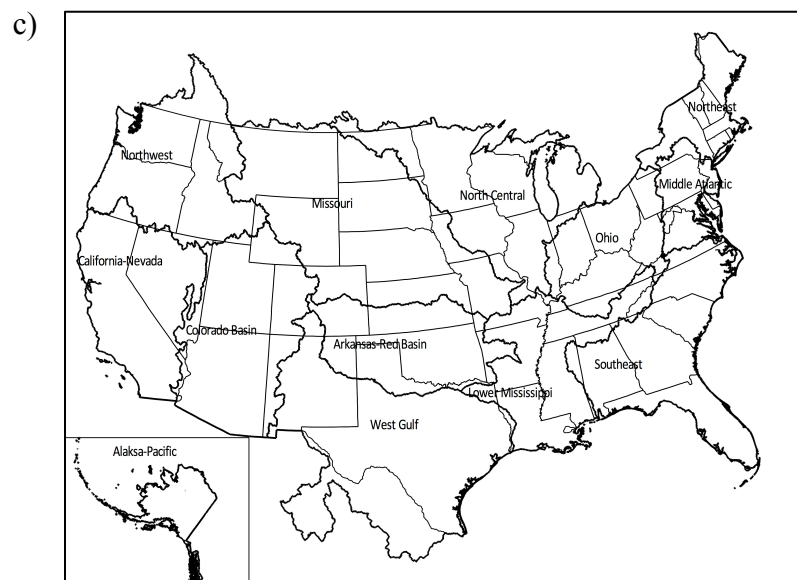
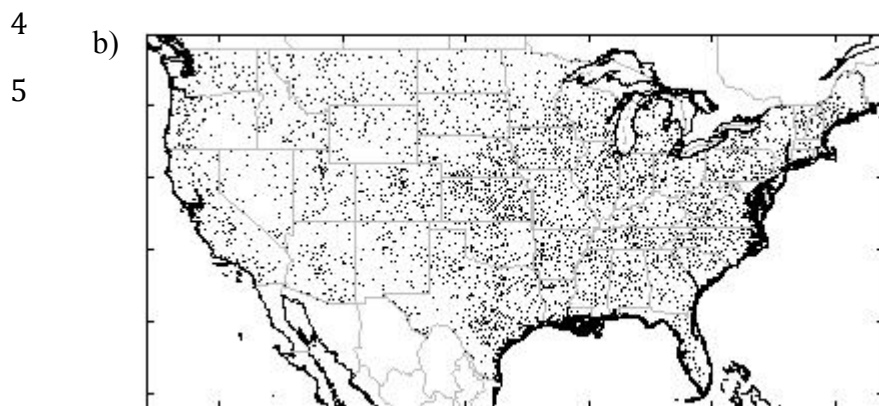
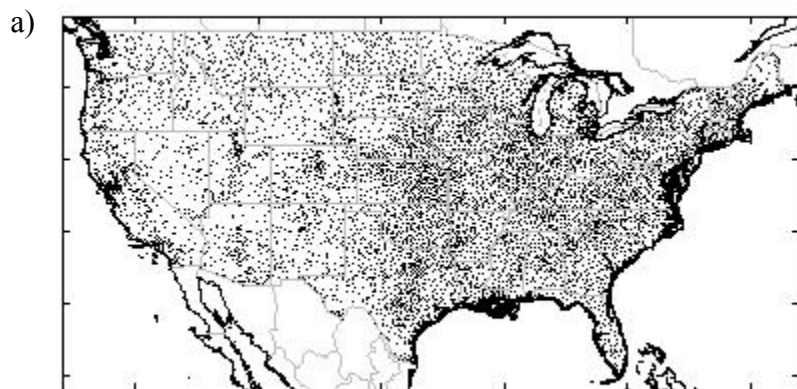
ID	GHCN -D	PRISM	Stage IV	TMPA	
				3B42	3B42RT
CONUS	2.47	2.42 [-2.2 0.98 0.98]*	2.31 [-6.4 0.93 0.93]*	2.52 [+2.1 1.00 0.83]*	2.62 [+6.1 0.99 0.36]*
ABRFC	2.13	2.06 [-3.0 0.97 0.99]	2.14 [+0.7 1.00 0.96]	2.27 [+6.9 1.06 0.96]*	2.40 [+12.5 1.12 0.94]*
CBRFC	0.89	0.90 [+0.7 0.99 0.87]	0.77 [-13.0 0.89 0.86]*	0.84 [-6.1 0.86 -0.02]	1.18 [+33.2 1.22 0.02]*
CNRFC	1.46	1.46 [+0.3 1.00 0.98]	1.32 [-9.7 0.91 0.92]	1.05 [-28.0 0.63 0.54]*	0.98 [-32.2 0.52 -0.10]*
LMRFC	3.75	3.64 [-2.8 0.97 0.84]*	3.48 [-7.3 0.93 0.54]*	3.87 [+3.2 1.03 0.26]*	3.90 [+3.9 1.0 -0.59]*
MARFC	3.28	3.17 [-3.4 0.97 0.89]*	3.12 [-5.0 0.95 0.63]*	3.34 [+1.6 1.01 -0.21]	2.78 [-15.2 0.84 -1.49]*
MBRFC	1.59	1.54 [-2.6 0.97 0.97]	1.59 [+0.4 1.00 0.87]	1.72 [+8.4 1.08 0.94]*	2.37 [+49.3 1.42 0.56]*
NCRFC	2.42	2.35 [-2.9 0.97 0.90]*	2.19 [-9.3 0.91 0.65]*	2.63 [+9.0 1.09 0.74]*	2.95 [+21.9 1.21 0.17]*
NERFC	3.44	3.38 [-1.8 0.98 0.89]	3.14 [-8.7 0.91 0.43]*	3.43 [-0.1 0.99 -0.88]	2.73 [-20.7 0.78 -1.42]*
NWRFC	2.28	2.36 [+3.6 1.03 0.97]	1.96 [-13.9 0.87 0.93]*	1.80 [-20.8 0.65 0.43]*	1.68 [-26.1 0.47 -3.58]*
OHRFC	3.28	3.20 [-2.3 0.98 0.89]*	3.09 [-5.8 0.94 0.45]*	3.44 [+4.9 1.05 0.42]*	3.35 [+2.2 1.02 0.13]
SERFC	3.58	3.47 [-3.1 0.97 0.84]*	3.36 [-6.2 0.93 0.45]*	3.68 [+2.7 1.02 -0.08]*	3.56 [-0.7 0.98 -0.08]
WGRFC	2.04	1.98 [-3.0 0.97 0.98]	1.89 [-7.4 0.93 0.94]*	2.11 [+3.2 1.03 0.96]	2.19 [+7.4 1.06 0.87]*

7

1 Table 3: Average rain rate (mm/day) and differences [%] between GHCN-D and other annual
2 precipitation estimates (PRISM, Stage IV, 3B42, 3B42RT) over CONUS and over each RFC for
3 winter (DJF) and summer (JJA). For each QPE datasets and season, the numbers in bold and
4 italic-bold indicate the upper and lower limits when compared to GHCN-D. The asterisk
5 indicates that the datasets are statistically different at the 5% significance level with respect to
6 surface observations.

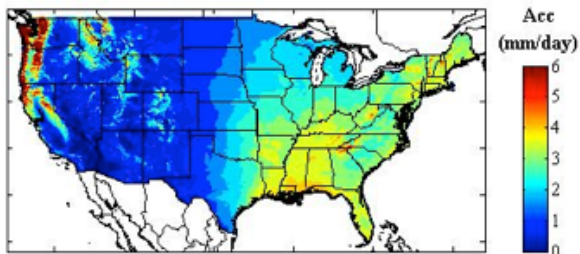
Season	ID	GHCN-D	PRISM	Stage IV	TMPA	
					3B42	3B42RT
DJF	CONUS	2.09	2.03 [-2.8]	1.89 [-9.5]*	2.09 [+0.1]	2.31 [+10.7]*
	ABRFC	1.17	1.14 [-2.4]	1.15 [-1.5]	1.28 [+9.2]	1.31 [+11.6]
	CBRFC	1.01	1.01 [-0.2]	0.86 [-14.8]*	0.83 [-17.4]*	1.32 [+30.4]*
	CNRFC	3.09	3.06 [-1.2]	2.72 [-12.2]	1.92 [-38.0]*	1.57 [-49.3]*
	LMRFC	3.77	3.64 [-3.5]*	3.37 [-10.6]*	4.03 [+6.8]*	4.12 [+9.1]*
	MARFC	2.60	2.44 [-5.9]*	2.54 [-2.2]	2.60 [+0.1]	2.32 [-10.4]*
	MBRFC	0.64	0.62 [-2.5]	0.60 [-4.9]	0.74 [+16.7]*	1.57 [+146.8]*
	NCRFC	1.35	1.30 [-4.0]	1.22 [-10.3]*	1.69 [+24.9]*	2.44 [+80.0]*
	NERFC	2.89	2.76 [-4.4]*	2.67 [-7.6]*	3.13 [+8.2]*	2.59 [-10.3]*
	NWRFC	3.54	3.60 [+1.8]	3.11 [-12.2]	2.44 [-31.1]*	2.51 [-29.0]*
	OHRFC	2.86	2.73 [-4.7]*	2.73 [-4.7]*	3.11 [+8.8]*	3.31 [+15.6]*
	SERFC	3.13	3.00 [-4.0]*	2.78 [-11.2]*	3.25 [+3.7]	3.00 [-4.3]
	WGRFC	1.51	1.51 [-0.8]	1.25 [-18.0]*	1.51 [+0.7]	1.59 [+4.5]
JJA	CONUS	2.73	2.65 [-3.0]*	2.64 [-3.3]*	2.85 [+4.4]*	3.32 [+21.5]*
	ABRFC	2.80	2.72 [-2.9]	2.94 [+5.2]*	3.00 [+7.3]*	3.45 [+23.2]*
	CBRFC	0.88	0.86 [-2.6]	0.77 [-13.3]*	0.93 [+5.3]	1.24 [+40.0]*
	CNRFC	0.17	0.17 [+0.6]	0.12 [-27.6]*	0.21 [+24.7]	0.33 [+91.8]*
	LMRFC	3.62	3.48 [-3.8]*	3.46 [-4.4]*	3.70 [+2.3]	3.92 [+8.2]*
	MARFC	3.63	3.51 [-3.5]*	3.38 [-6.9]*	3.81 [+4.8]*	3.71 [+2.1]
	MBRFC	2.37	2.30 [-3.0]	2.56 [+8.4]*	2.55 [+7.7]*	3.81 [+60.9]*
	NCRFC	3.31	3.22 [-2.6]*	3.02 [-8.7]*	3.51 [+6.1]*	4.33 [+31.0]*
	NERFC	3.78	3.68 [-2.5]	3.39 [-10.2]*	3.71 [-1.9]	3.64 [-3.7]*
	NWRFC	0.82	0.84 [+2.1]	0.66 [-19.1]*	0.81 [-1.7]	0.84 [+2.4]
	OHRFC	3.45	3.36 [-2.5]*	3.20 [-7.2]*	3.59 [+4.0]*	3.90 [+13.1]*
	SERFC	4.53	4.36 [-3.7]	4.41 [-2.6]	4.66 [+2.8]	5.00 [+10.3]*
	WGRFC	2.39	2.30 [-3.7]	2.39 [-0.1]	2.48 [+3.8]	2.69 [+12.5]*

1 Figure 1: a) Locations of the GHCN-Daily rain gauges locations over CONUS: a) Total 8815
2 rain gauges, and b) The 4075 rain gauges reporting at least 90% of the time during the period
3 2002-2012. c) National Weather Service (NWS) 12 River Forecast Centers (RFCs).

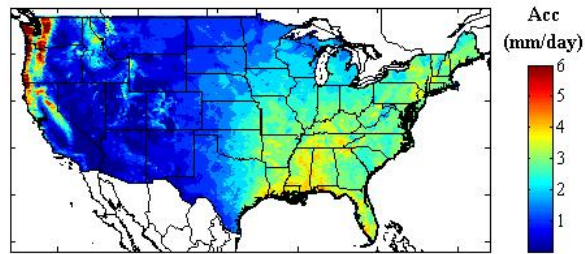


1 Figure 2: Annual average precipitation derived from: a) PRISM, b) Stage IV, c) TMPA 3B42,
2 and d) TMPA 3B42RT for the period 2002-2012.

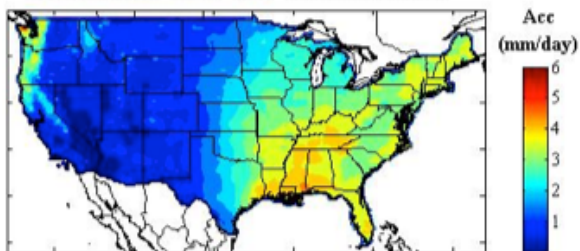
3 a) PRISM (0.04°x0.04°): Annual 2002-2012



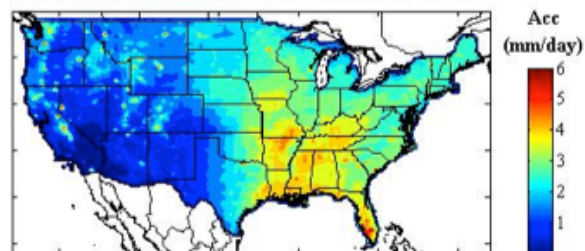
b) StIV (0.04°x0.04°): Annual 2002-2012



c) TMPA (0.25°x0.25°): Annual 2002-2012



d) TMPA RT (0.25°x0.25°): Annual 2002-2012

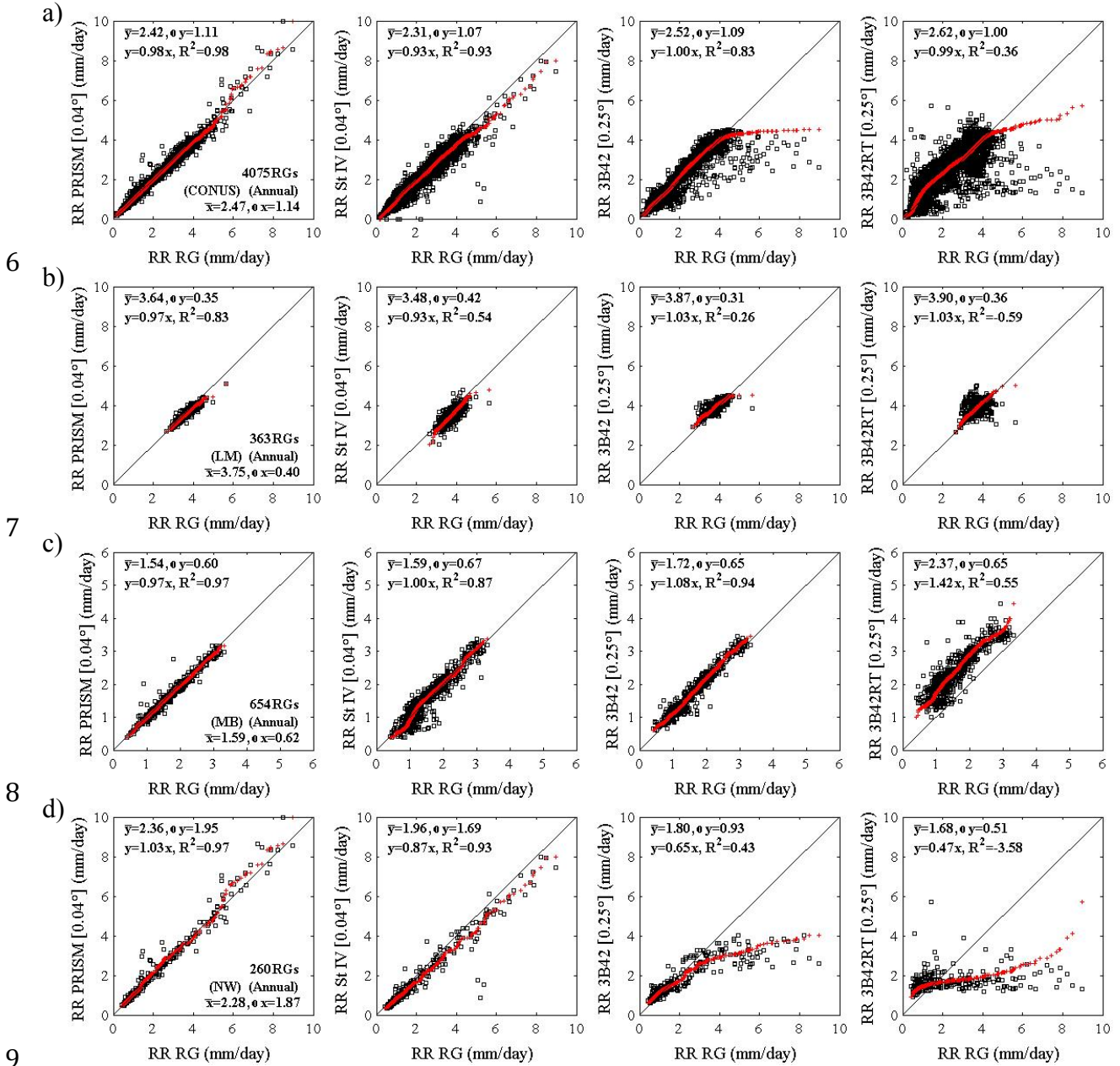


3

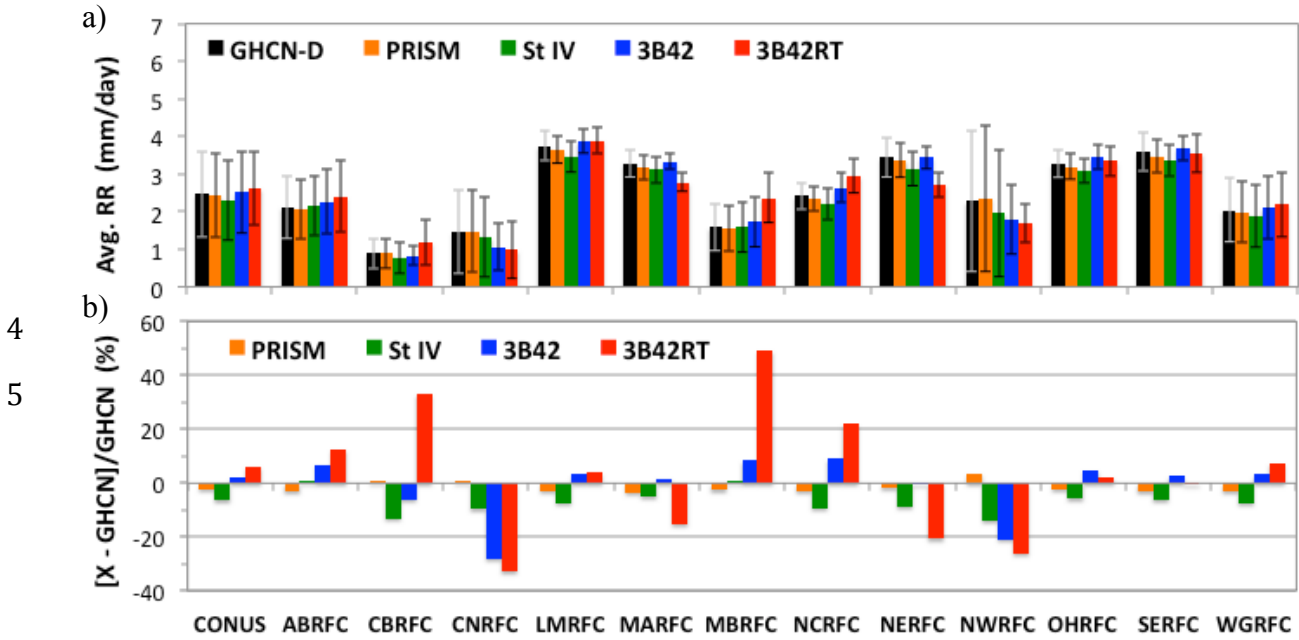
4

5

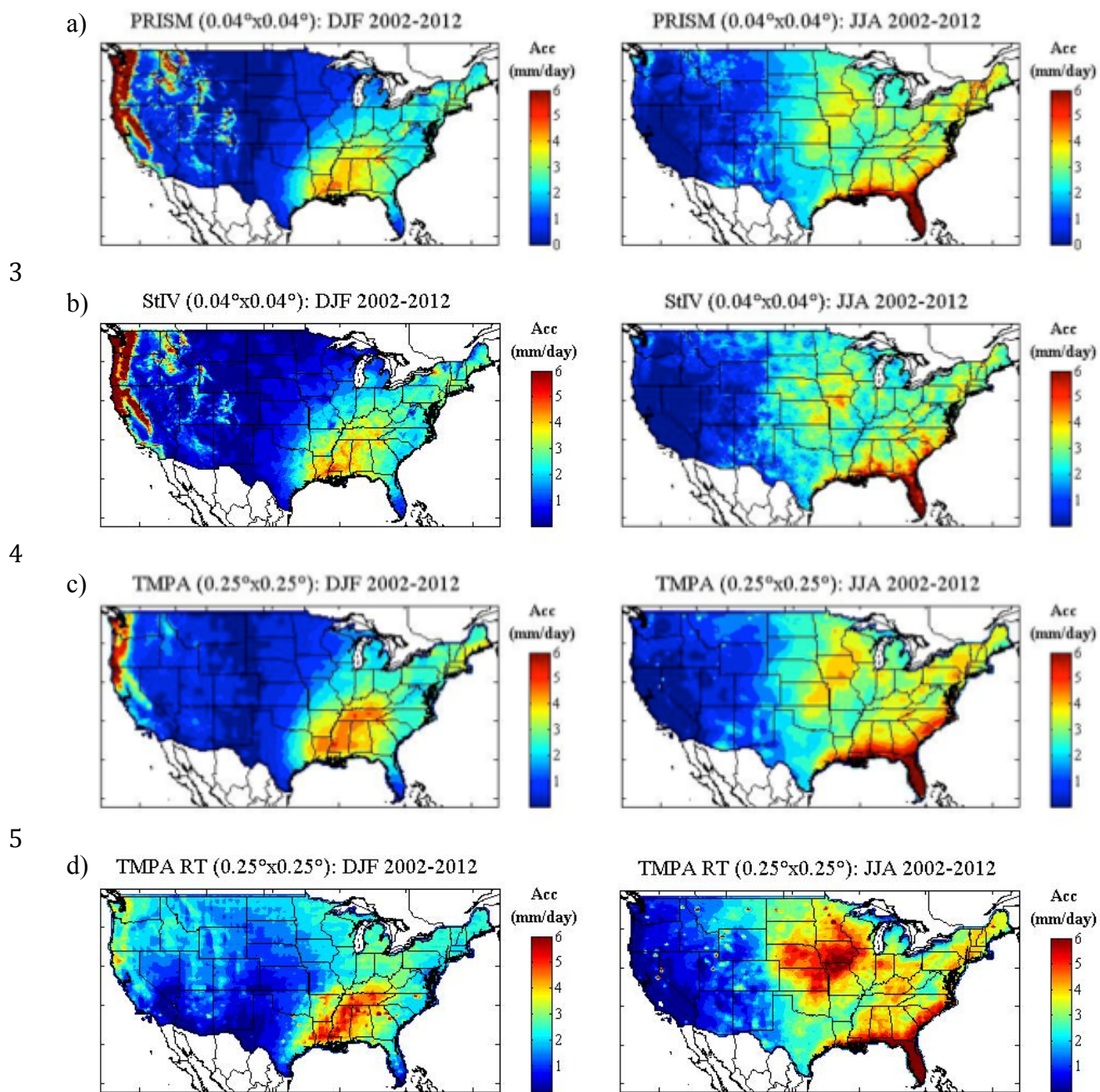
1 Figure 3: Scatterplots (black) and Quantile-Quantile (red) plots for annual precipitation derived
 2 from PRISM, Stage IV, TMPA 3B42, and TMPA 3B42RT when compared to GHCN-Daily
 3 network for: a) CONUS, b) Lower Mississippi River Basin (LM), c) Missouri Basin River (MB),
 4 and d) Northwest (NW) for the period 2002-2012. Please note that for row c), the scale is
 5 different then for rows a), b), and d).



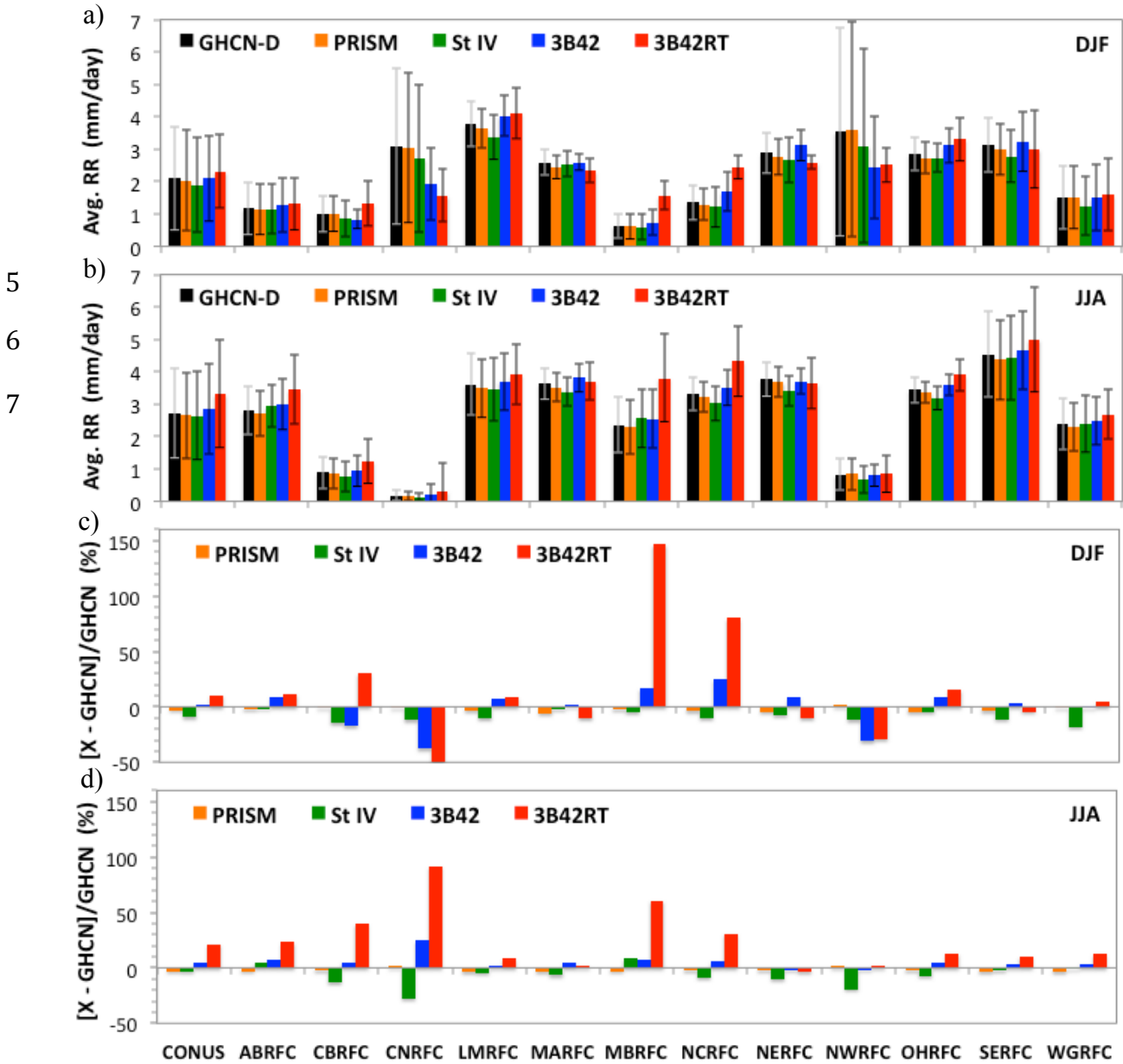
1 Figure 4: Average annual precipitation derived from GHCN-D, PRISM, Stage IV, TMPA 3B42,
 2 and TMPA 3B42RT for the different RFCs. Differences (%) with respect to GHCN-D surface
 3 measurements.



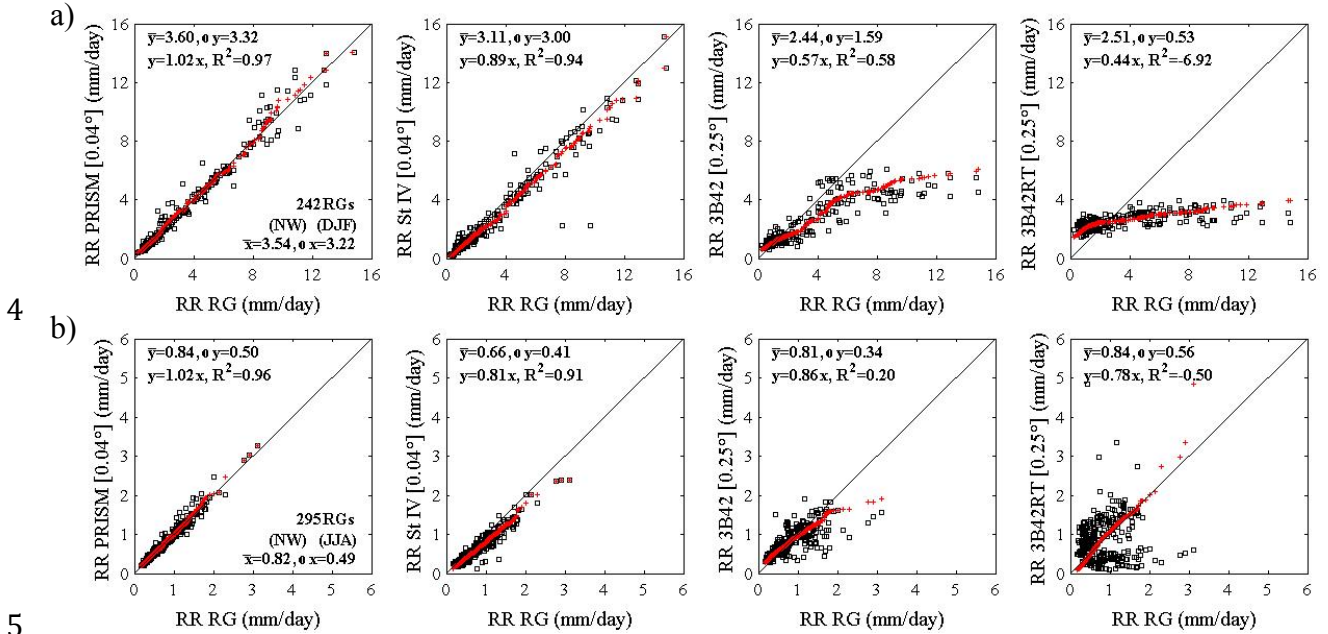
1 Figure 5: Winter (DJF: Left Column) and summer (JJA: Right Column) precipitation derived
2 from: a) PRISM, b) Stage IV, c) TMPA 3B42, and d) TMPA 3B42RT for the period 2002-2012.



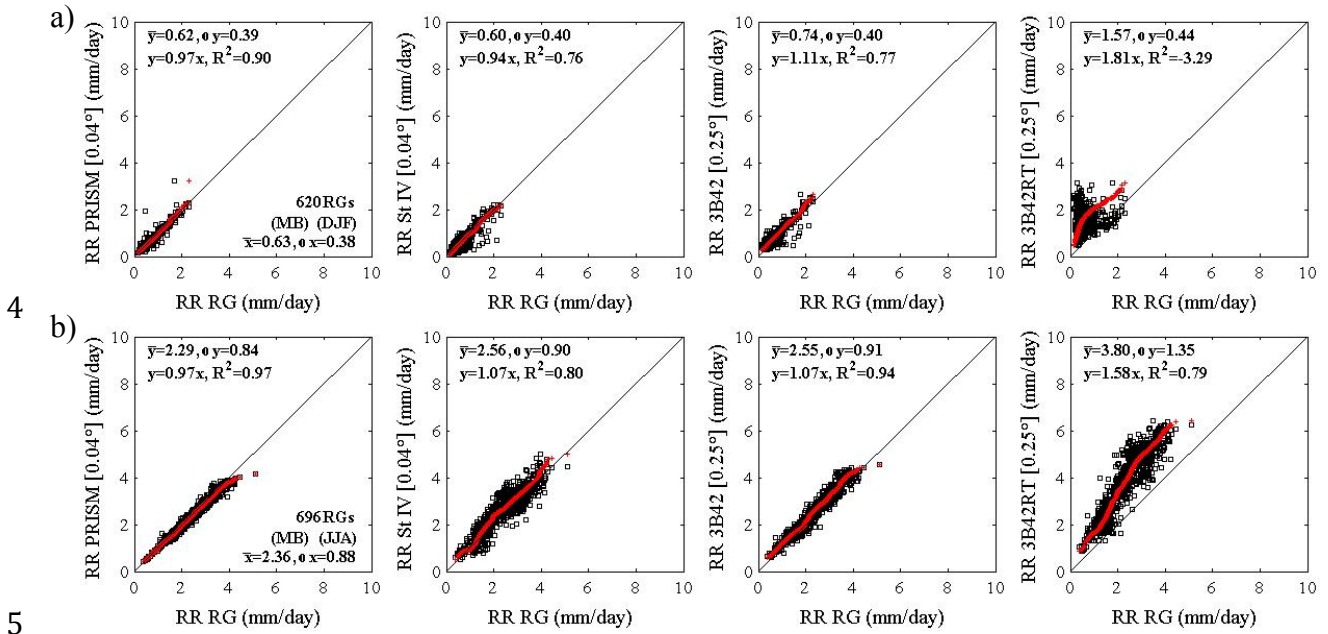
1 Figure 6: Seasonal rain-rate derived from GHCN-D, PRISM, Stage IV, TMPA 3B42, and TMPA
 2 3B42RT for each RFC and for: a) Winter (DJF), and b) Summer (JJA). Differences between
 3 GHCN-D and PRISM, Stage IV, TMPA 3B42, and TMPA 3B42RT for: c) Winter (DJF), and d)
 4 Summer (JJA).



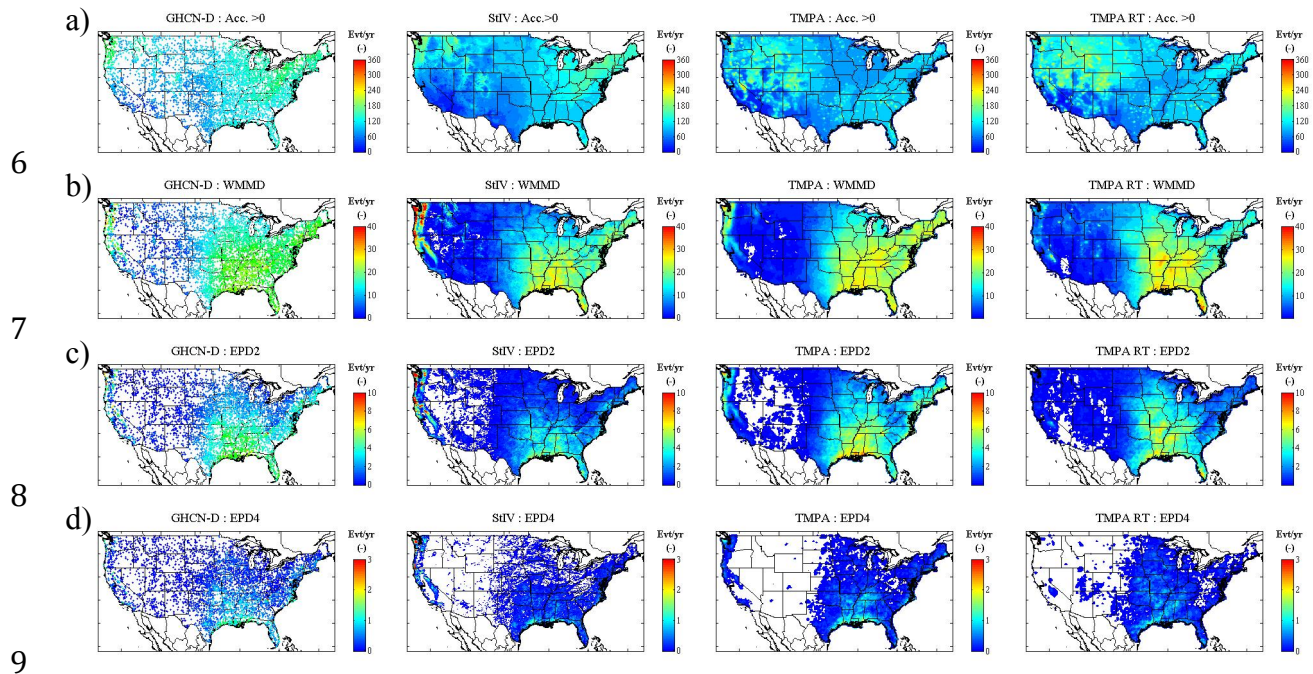
1 Figure 7: Scatterplots (black) and Q-Q plots (red) for the seasonal rain-rate for PRISM, Stage IV,
 2 TMPA 3B42, and TMPA 3B42RT for: a) Winter (DJF), and b) Summer (JJA) over Northwest
 3 (NW).



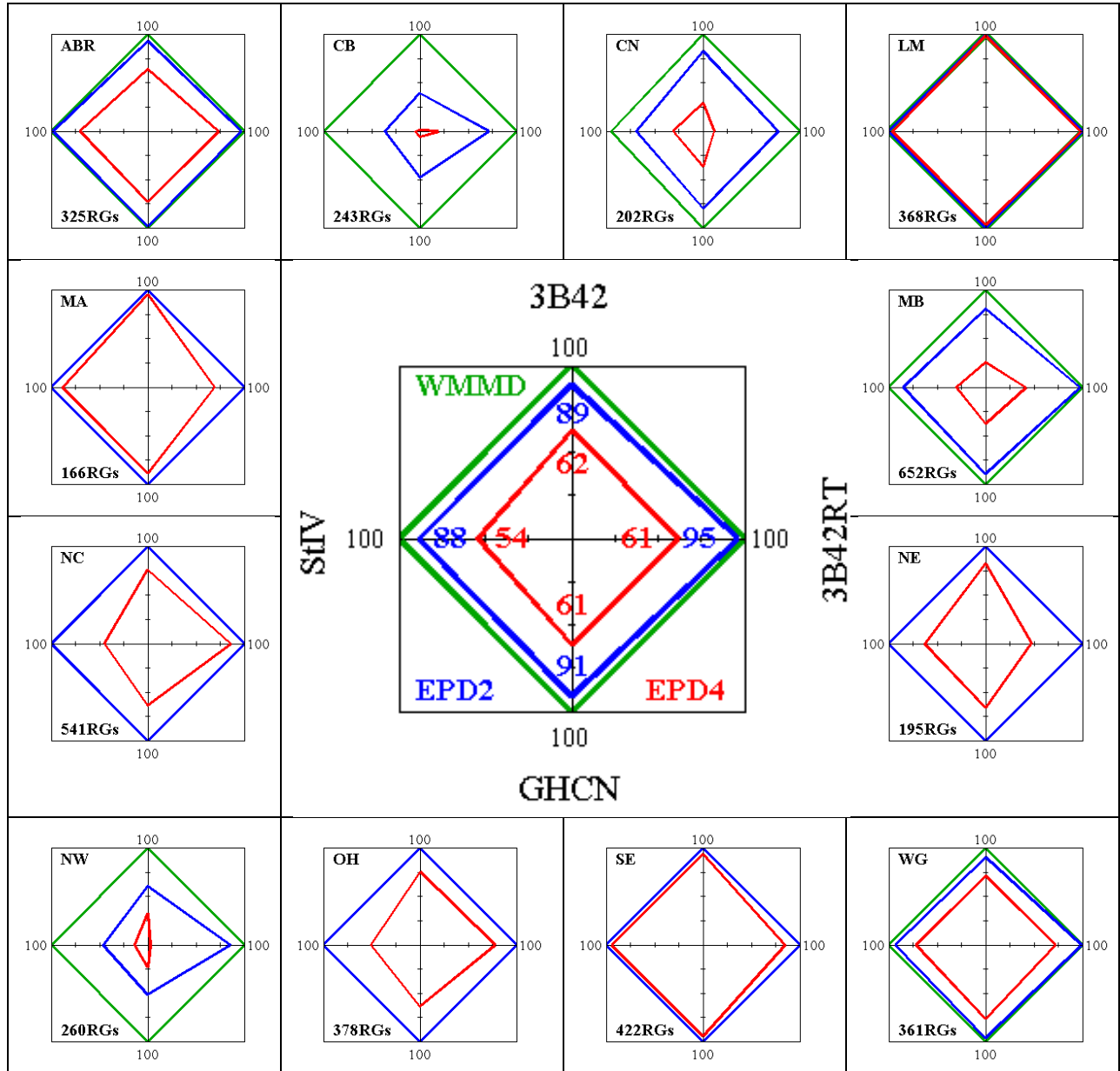
- 1 Figure 8: Scatterplots (black) and Q-Q plots (red) for the seasonal rain-rate for PRISM, Stage IV,
- 2 TMPA 3B42, and TMPA 3B42RT for: a) Winter (DJF), and b) Summer (JJA) over the Missouri
- 3 Basin River (MB).



1 Figure 9: a) Number of rainy days ($RR > 0$ mm/day), b) Wet Millimeter Days ($RR > 17.8$
 2 mm/day: WMMD), c) Precipitation Days with accumulation greater than 2 in day^{-1} ($RR > 50.8$
 3 mm/day: EPD2), and d) Precipitation Days with accumulation greater than 4 in day^{-1} ($RR >$
 4 101.6 mm/day: EPD4) for GHCN-D (first column), Stage IV (second column), TMPA 3B42
 5 (third column), and TMPA 3B42RT (fourth column).

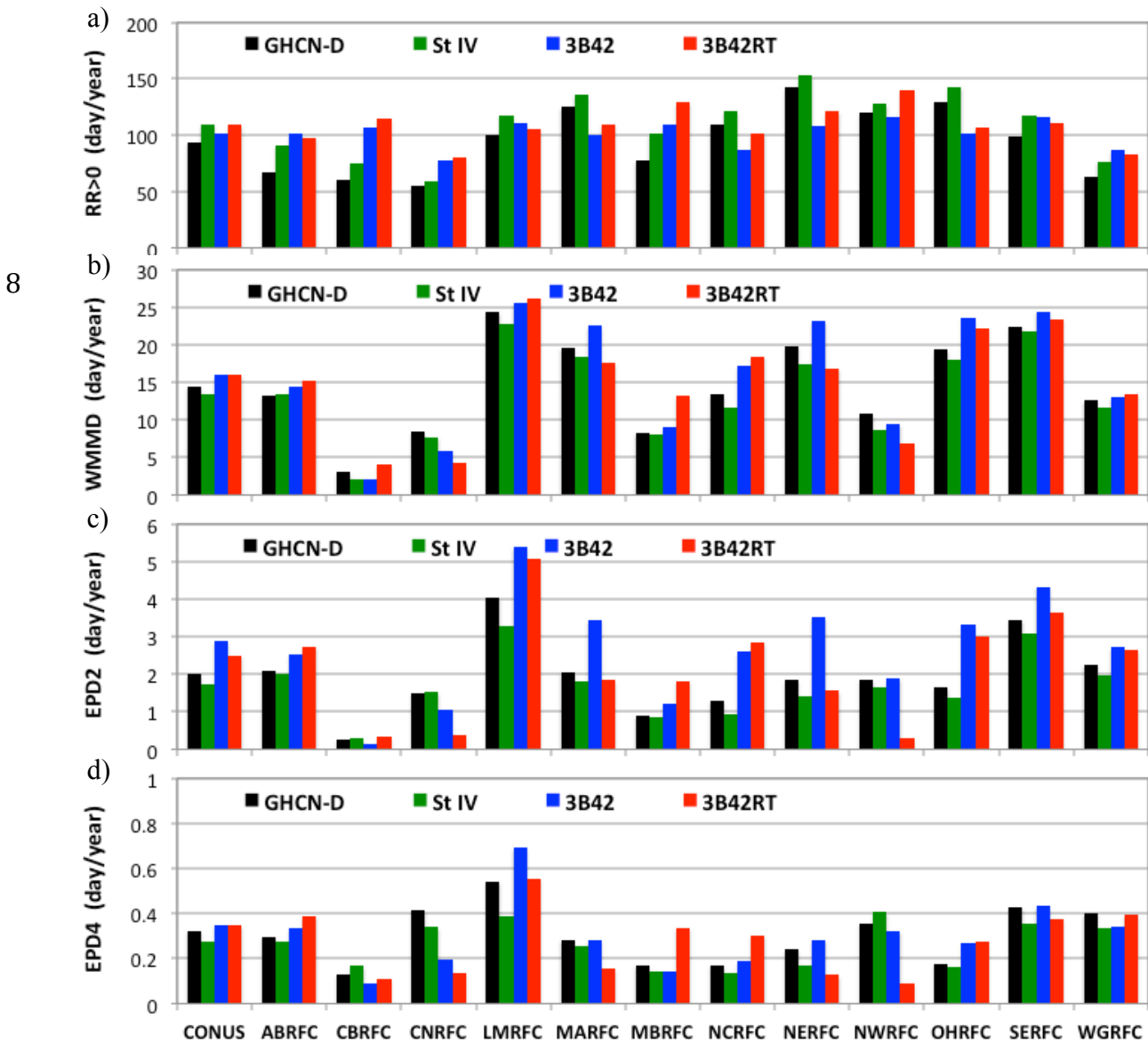


- 1 Figure 10: Proportion (%) of stations (GHCN-D) and corresponding pixel (Stage IV, TMPA 3B42, TMPA 3B42RT) experiencing WMMD, EPD2, and EPD4 over CONUS (central figure)
- 2 3B42, TMPA 3B42RT) experiencing WMMD, EPD2, and EPD4 over CONUS (central figure)
- 3 and for the 12 River Forecast Centers (border figures).

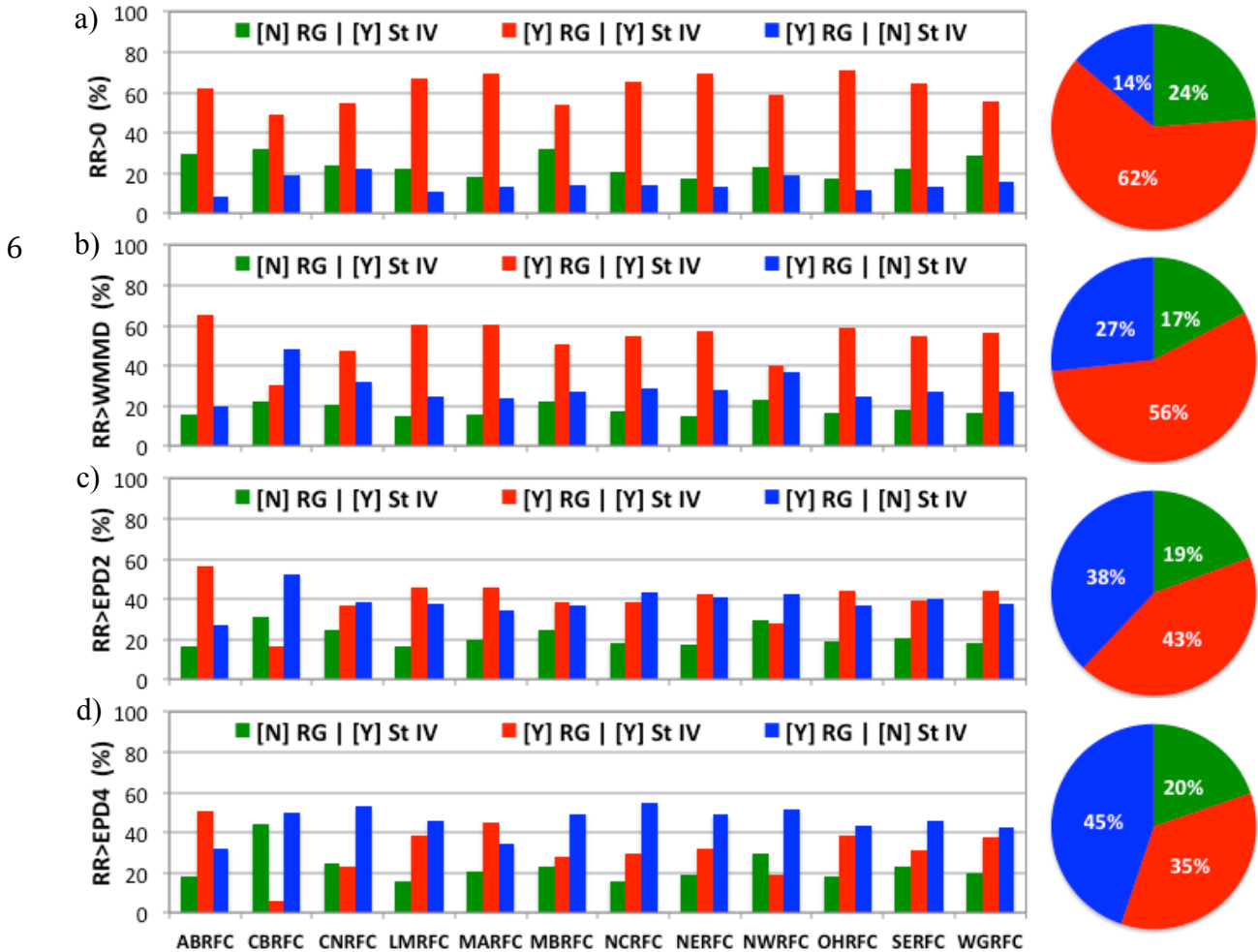


4

1 Figure 11: Average number of: a) Rainy days, b) Wet Millimeter Days (WMMD) i.e.
 2 precipitation days with accumulation greater than 17.8 mm/day, c) Precipitation Days with
 3 accumulation greater than 2 in day⁻¹ (EPD2), and d) Precipitation Days with accumulation
 4 greater than 4 in day⁻¹ (EPD4) for GHCN-D, Stage IV, TMPA 3B42, and TMPA 3B42RT over
 5 CONUS and for the 12 River Forecast Centers (RFCs). Data are for the period 2002-2012. The
 6 average number of days is normalized by the number of locations experiencing at least one event
 7 (Fig. 10).



1 Figure 12: Contingency as a function of the daily threshold selected: a) RR>0, b) RR>WMMD,
 2 c) RR>EPD2, and d) RR>EPD4 for rainfall observed simultaneously at the rain gauge and at the
 3 radar pixel [YY: red], and successively at the rain gauge only [YN: blue], or at the radar pixel
 4 only [NY: green] over CONUS (circle) and for the 12 RFCs (bars). Data are for the period
 5 2002-2012.



1 Figure 13: Contingency analysis at the rain gauge site with respect to the daily rainfall
 2 accumulation: a) $RR > 0$, b) $RR > WMMD$, c) $RR > EPD2$, and d) $RR > EPD4$ for rain observed
 3 at the radar pixel only (first column), simultaneously at the rain gauge and radar (second
 4 column), and at the rain gauge only (third column). e) and f) Same as c) and d) but only
 5 displaying single event occurrence over the period 2002-2012.

